Photo-neutron Reaction on ^{208}Pb Measured at NewSUBARU

I. Gheorghe et al., https://arxiv.org/pdf/2403.11547

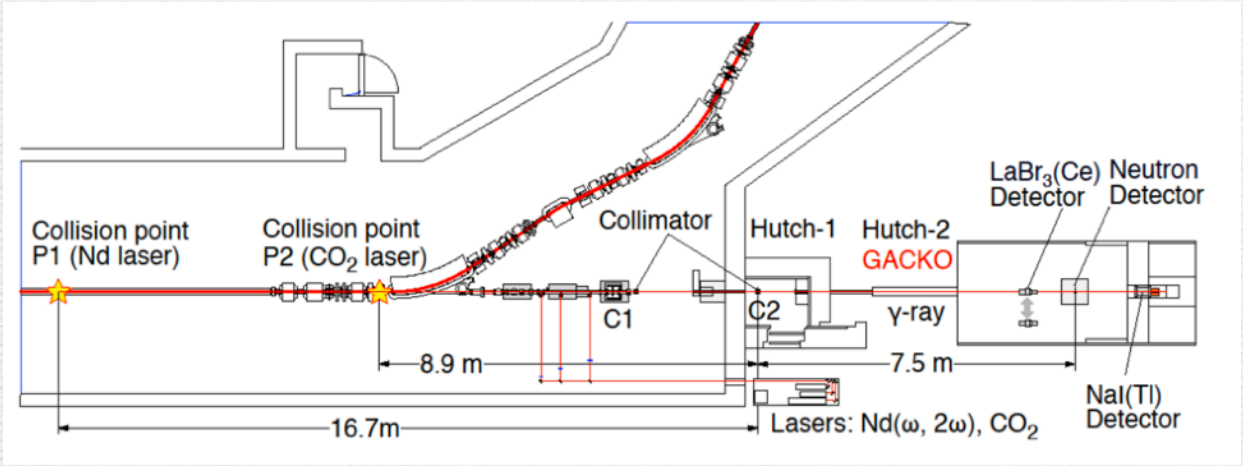

GACKO at NewSUBARU

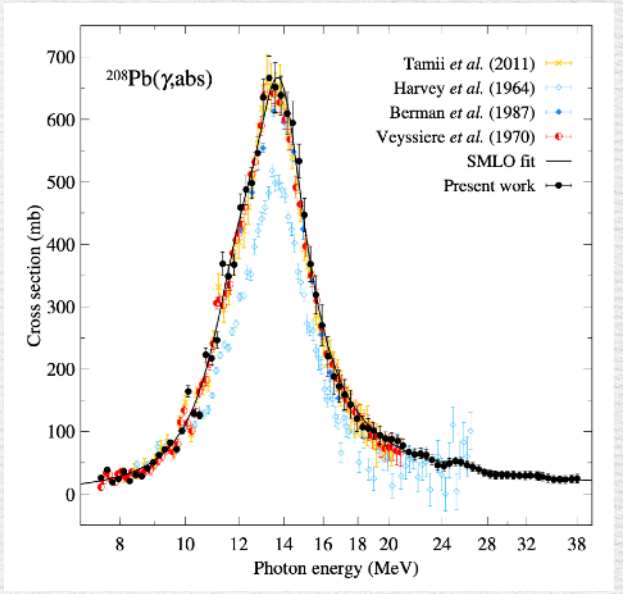

(γ,abs)

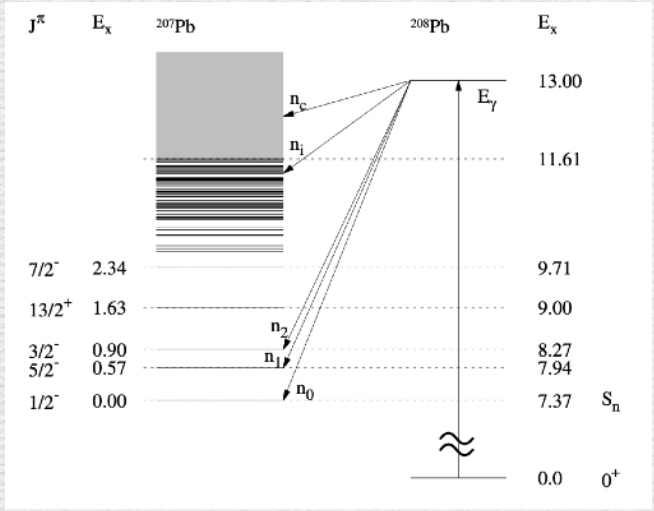

Photo-neutron Reaction

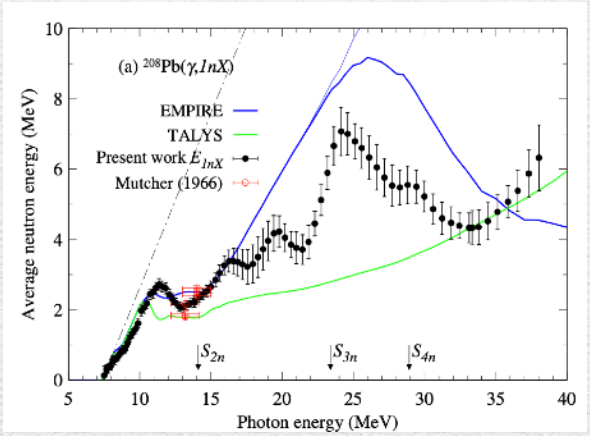

RCNP核理1aグループ勉強会 2024.6.3 by A. Tamii

Abstract

Photoneutron cross section measurements on ^{208}Pb in the Giant Dipole Resonance region

I. Gheorghe,[1,*] S. Goriely,[2] N. Wagner,[3] T. Aumann,[3,4,5] M. Baumann,[3] P. van Beek,[3] P. Kuchenbrod,[3] H. Scheit,[3] D. Symochko,[3] T. Ari-izumi,[6] F.L. Bello Garrote,[7] T. Eriksen,[7] W. Paulsen,[7] L.G. Pedersen,[7] F. Reaz,[7] V. W. Ingeberg,[7] S. Belyshev,[8] S. Miyamoto,[9] and H. Utsunomiya[10,†]

[1]*National Institute for Physics and Nuclear Engineering, Horia Hulubei (IFIN-HH), 30 Reactorului, 077125 Bucharest-Magurele, Romania*
[2]*Institut d'Astronomie et d'Astrophysique, Université Libre de Bruxelles, Campus de la Plaine, CP-226, 1050 Brussels, Belgium*
[3]*Institut für Kernphysik, Technische Universität Darmstadt, Darmstadt, 64289, Germany*
[4]*GSI Helmholtzzentrum für Schwerionenforschung, 64291 Darmstadt,Germany*
[5]*Helmholtz Forschungsakademie Hessen für FAIR (HFHF), GSI Helmholtzzentrum für Schwerionenforschung, 64291 Darmstadt, Germany*
[6]*Konan University, Department of Physics, 8-9-1 Okamoto, Higashinada, Kobe 658-8501,Japan*
[7]*Department of Physics, University of Oslo, N-0316 Oslo, Norway*
[8]*Lomonosov Moscow State University, Faculty of Physics, 119991 Moscow, Russia*
[9]*Laboratory of Advanced Science and Technology for Industry, University of Hyogo, 3-1-2 Kouto, Kamigori, Ako-gun, Hyogo 678-1205, Japan*
[10]*Konan University, Department of Physics, 8-9-1 Okamoto, Higashinada, Kobe 658-8501, Japan*

(Dated: March 19, 2024)

Photoneutron reactions on ^{208}Pb in the Giant Dipole Resonance energy region have been investigated at the γ-ray beam line of the NewSUBARU facility in Japan. The measurements made use of quasi-monochromatic laser Compton backscattering γ-ray beams in a broad energy range, from the neutron threshold up to 38 MeV, and of a flat-efficiency moderated ^{3}He neutron detection system along with associated neutron-multiplicity sorting methods. We report absolute cross sections and mean photoneutron energies for the ^{208}Pb(γ, inX) reactions with $i = 1$ to 4. The fine structure present in the ^{208}Pb(γ, n) cross sections at incident energies lower than 13 MeV has been observed. The photoabsorption cross section has been obtained as the sum of the (γ, inX) reaction cross sections. By reproducing the measured ring-ratio values at excitation energies below the two neutron separation energy, we were able to extract estimations on the ^{208}Pb(γ, n) photoneutron energy spectra and on the partial photoneutron cross sections for leaving the residual ^{207}Pb in its ground and first two excited states. The present results are compared with data from the literature and statistical model calculations.

Background of the Research

Photo-Nuclear Reactions

are important as a fundamental reaction for studying

- Nuclear structure/reaction studies
- Astro-nuclear physics, particle physics, detector response
- Applications
  - Radiation shield, decommissioning, reactions in nuclear reactors
  - Photo-activation analysis, nondestructive inspection
  - γ-imaging、CT-diagnostics、biological effects
  - Homeland security、inspection of fission or explosive material
  - Medical RI production by photo-irradiation
  - Nuclear reaction/gamma radiation in thunder volts

Photo-Nuclear Reactions

A photon interacts protons in the target nuclei

→ excites the Iso-Vector Giant Dipole Resonance (IVGDR)

$E_x \simeq$ 10-30 MeV

by electric dipole (*E1*) interaction

IV Giant Dipole Resonance

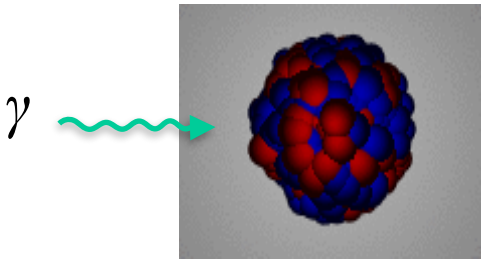

Photo-absorption cross section dominated by the electric dipole excitation of nuclei.

$$\sigma_{\text{abs}} = \frac{16\pi^3}{9}\alpha E_\gamma \frac{dB(E1)}{dE_\gamma}$$

σ_{abs} : photo-absorption cross section

$B(E1)$: electric-dipole reduced transition probability

E_γ : photon-energy = nuclear excitation energy

α : fine structure constant

PANDORA Project

Systematic Measurement on Photo-Absorption C.S. and n, p, α, γ decays for **light** stable nuclei

- *E1* excitation strength distribution
- n, p, α, γ decay branching ratios
- from light to A~60 for stable nuclei

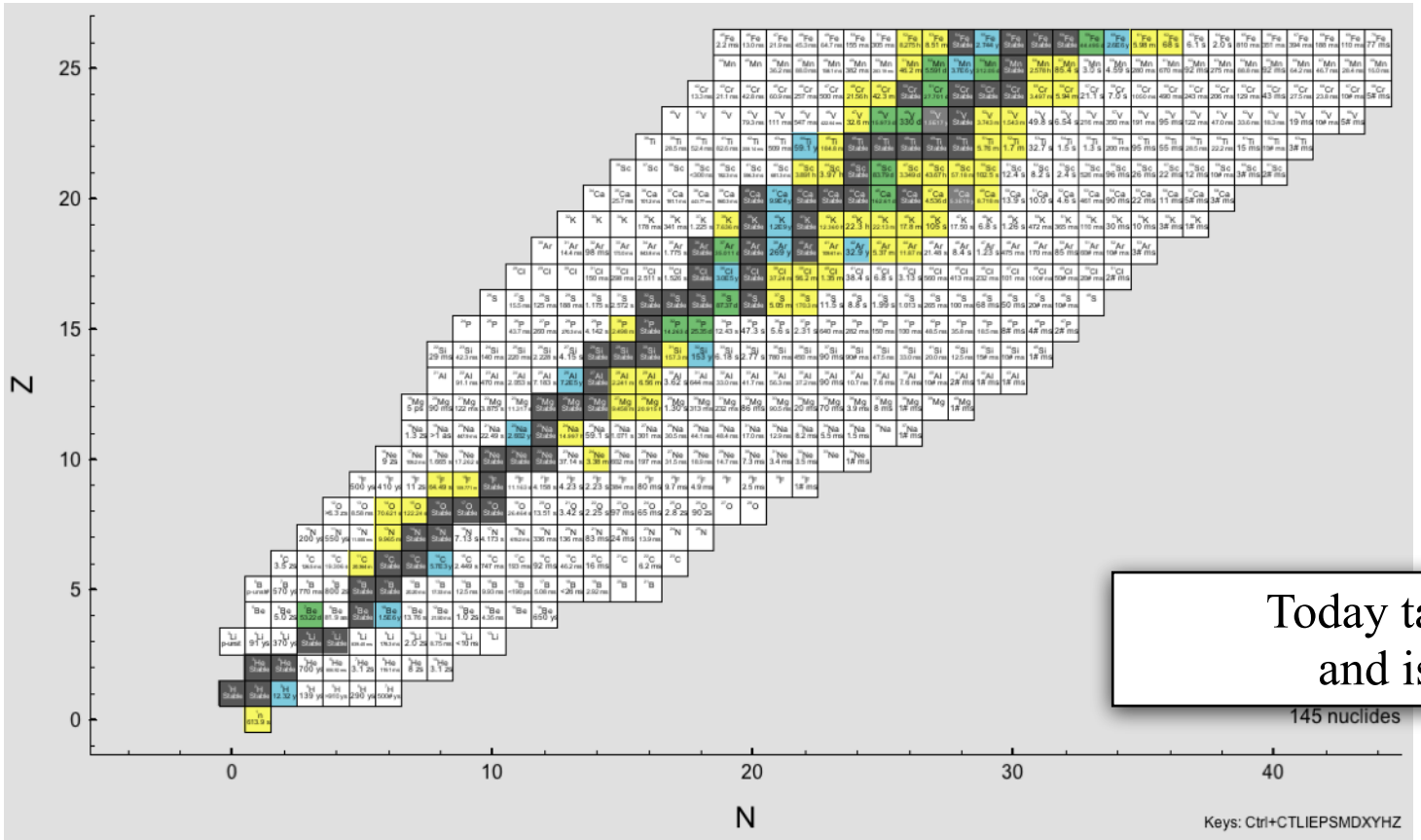

Today target ^{208}Pb
and is heavy.

Photo-absorption cross section of heavy nuclei

Being studied since the discovery of IVGDR

Shape of IVGDR:
well described by a single Lorentzian for spherical nuclei

$\sigma_{\mathrm{abs}} \simeq (\gamma, xn)$ cross sections for heavy nuclei

p and other charged particle decay
negligibly small due to Coulomb barrier

direct γ decay from IVGDR is ~1%

Beene *et al*., PRC39, 1307 (1989)

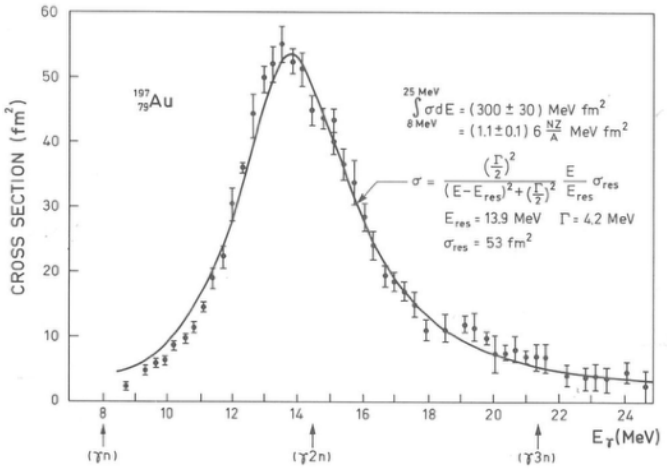

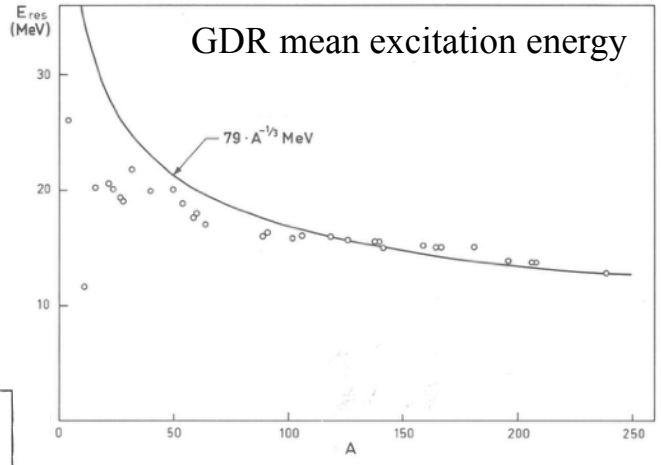

Bohr and Mottelson

Ratio to the TRK sum rule

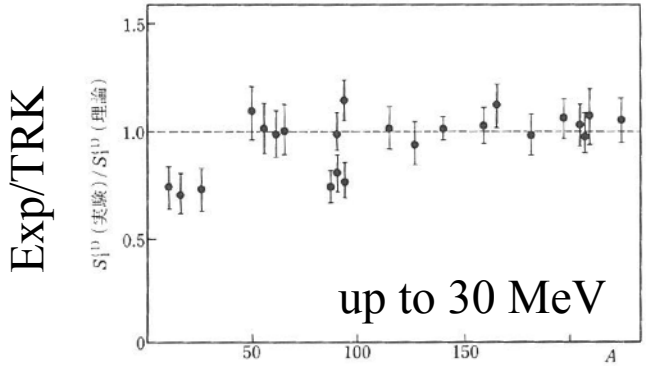

Electric Dipole Response of Nuclei

Electric dipole moment

$$p = \alpha_D \times E$$

α_D: electric dipole polarizability

The **restoring force** originates from the **symmetry energy.**

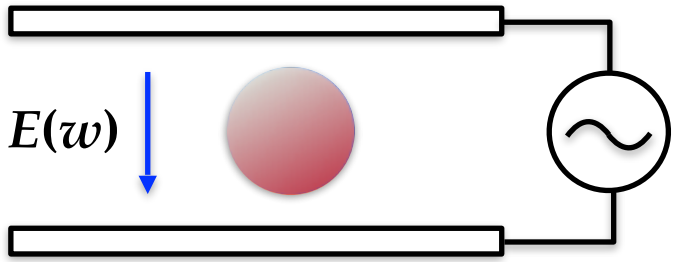

dielectric material
in an oscillating electric field

(E1) photo-absorption cross section

E1 reduced transition probability

$$\sigma_{\rm abs}^{E1} = \frac{16\pi^3 \alpha \omega}{9} \frac{dB(E1)}{d\omega}$$

Inversely energy-weighted sum-rule

$$\alpha_D = \frac{\hbar c}{2\pi^2} \int \frac{\sigma_{\rm abs}^{E1}}{\omega^2} d\omega = \frac{8\pi}{9} \int \frac{dB(E1)}{\omega}$$

A.B. Migdal: 1944

Constraints on Symmetry Energy (J and L)

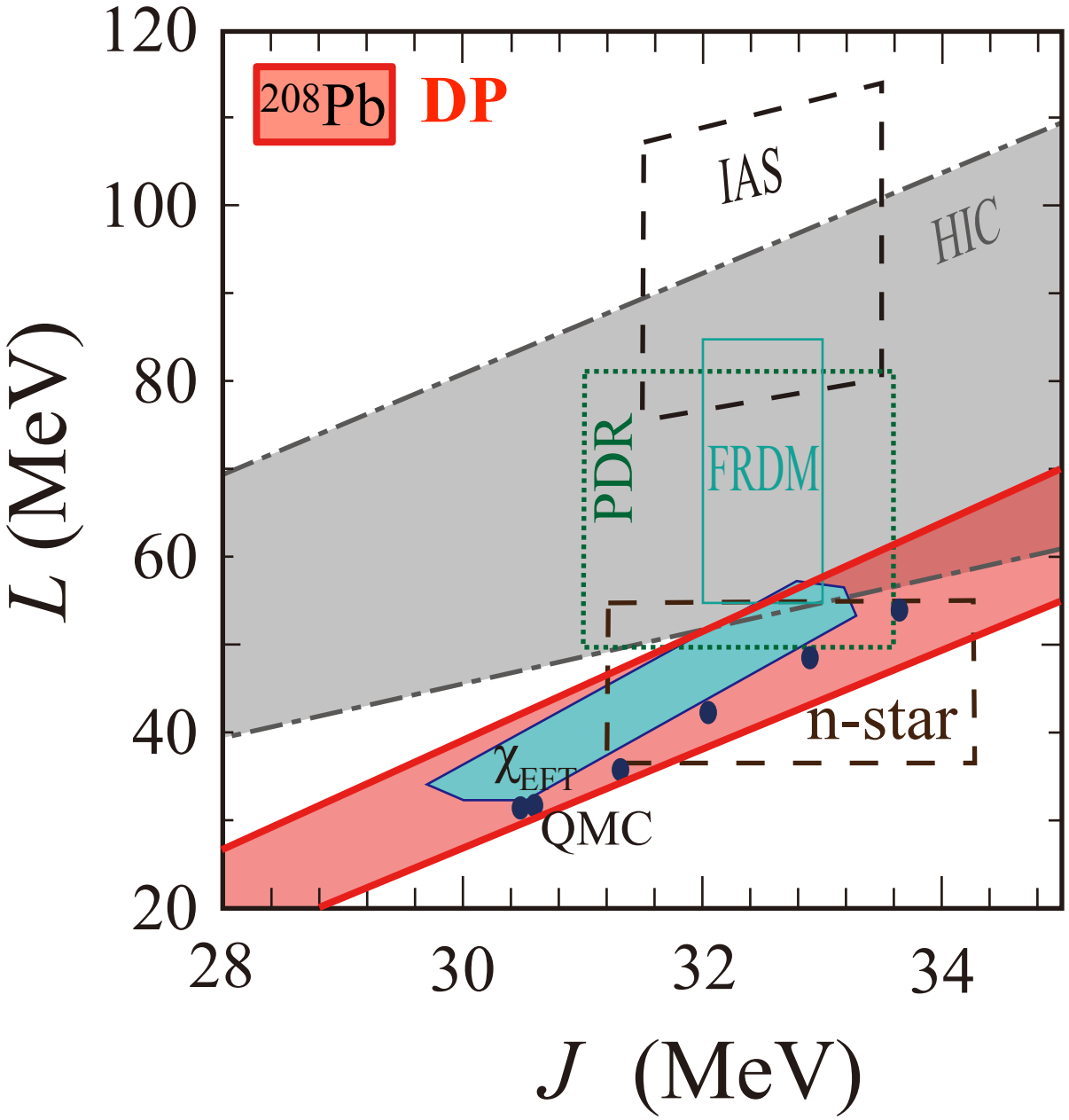

Nuclear EOS neglecting Coulomb

$$\frac{E}{A}(\rho,\delta)=\frac{E}{A}(\rho,0)+S(\rho)\delta^2+\cdots$$

$$\delta\equiv\frac{\rho_n-\rho_p}{\rho_n+\rho_p}$$

Symmetry energy

$$S(\rho)=J+\frac{L}{3\rho_0}(\rho-\rho_0)+\ldots$$

Why are the available data so inaccurate?

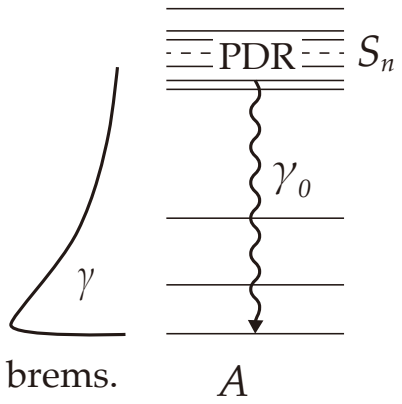

Bremsstrahlung gamma
+ γ-decay or activation measurement

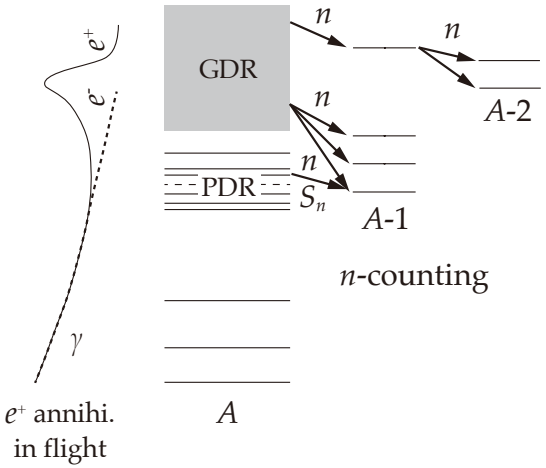

Positron annihilation in flight
+neutron counting

historical methods

A. Bracco, E.G. Lanza, AT, PPNP **106**, 360 (2019)

- **continuous energy spectrum** of Bremsstrahlung gamma-rays

  large systematic uncertainty by taking a **subtle difference** of different electron energies

  gamma-decay measurement only detects transitions to the ground state

- positron annihilation in flight

  needs to take **difference between e+ and e-** for cancelling atomic reactions

  flat *n* detection efficiency against *n* energy **is assumed** in the neutron counting

- charged particle decay measurement is difficult due to **low gamma intensity** and **thick target**
- **bad energy resolution** ≳ 500 keV

Modern Experimental Methods

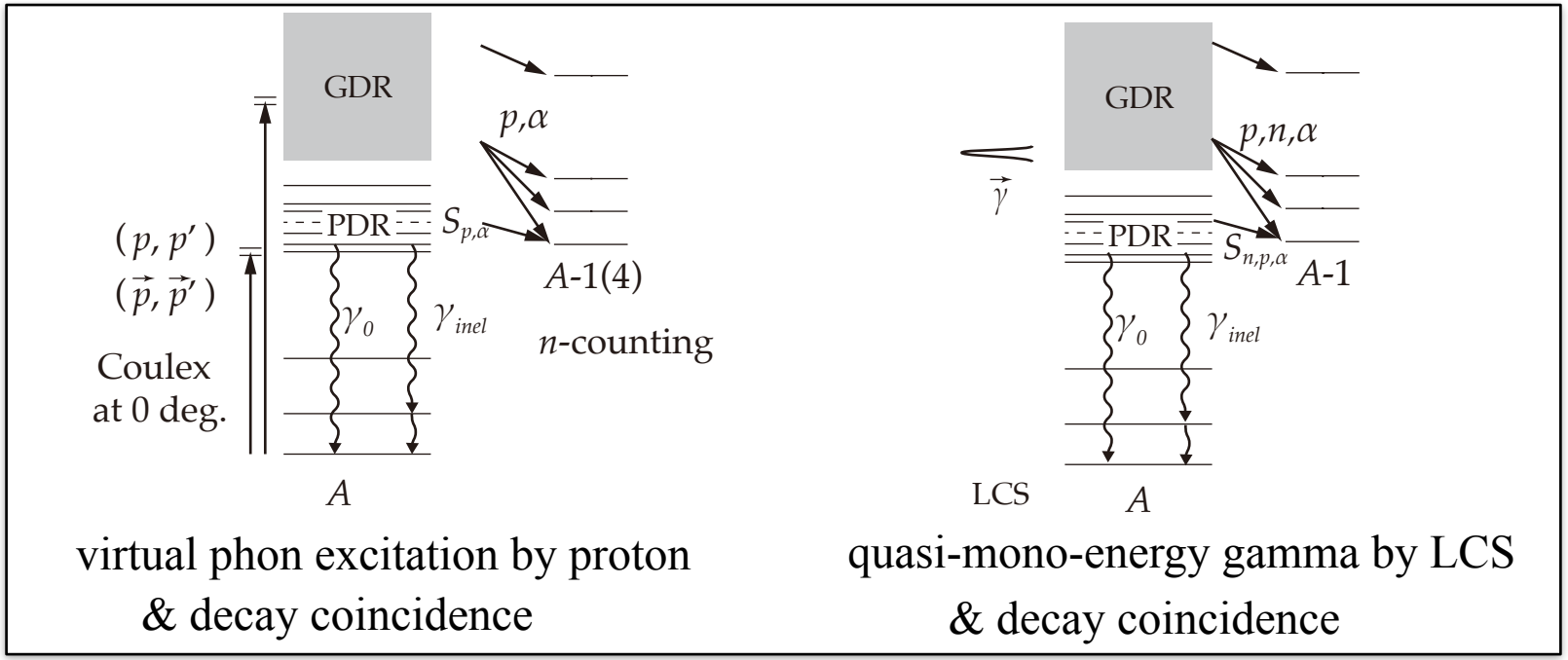

A. Bracco, E.G. Lanza, AT, PPNP **106**, 360 (2019)

- **virtual photon excitation** (proton Coulex) at RCNP and iThemba LABS

  Tag of excitation energy by scattered proton. Sensitive to **total photo-absorption c.s.**

  Good energy resolution of ~30 keV

  distribution

  C.S. is large, applicable to **isotopically enriched target** and **charged particle decays**

- **real photon excitation** by LCS gamma at ELI-NP

  absolute c.s.

  high-intensity, applicable to **isotopically enriched target** and **charged particle decays**

  Good energy resolution of ~50 keV by **quasi-mono-energetic** LCS beam

  Precise absolute c.s. and ***n* decay**

Probes for the Electric Dipole Response of Nuclei

1. Virtual photon excitation
   (Coulomb excitation)
   - proton inelastic scattering at 0 deg.

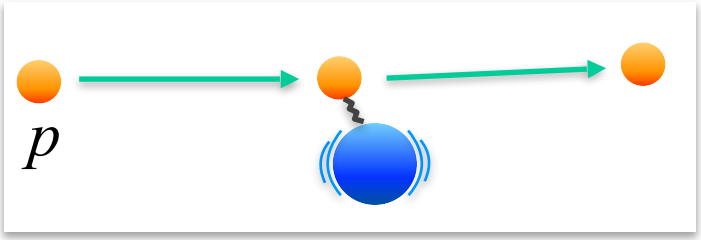

Proton beams at RCNP
and iThemba LABS

dominantly electric excitation: req. decomposition
E_x distribution is obtained in one shot
sensitive to the total strength

2. Real photon absorption
   - (γ,γ') Nuclear Resonance Fluorescence
   - (γ,n), (γ,2n), (γ,p), … photodisintegrations

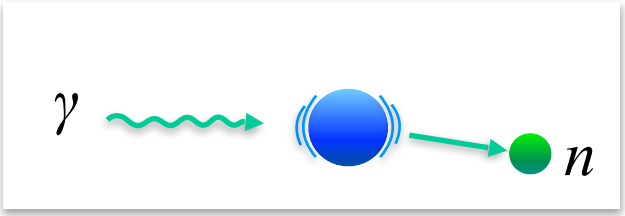

Real γ-beam at ELI-NP

at NewSUBARU

pure EM probe by quasi-monoenergetic γ
precise absolute strength
partial strength for each decay channel including *n*
clear selection of E1 and M1 (polarized-gamma)

Symmetry uncertainties in (γ,xn) data

^{232}Th, and ^{238}U. It was found that the $(\gamma, 1n)$ cross sections from Saclay tend to be larger than the Livermore data by up to 100%, while Livermore gives larger $(\gamma, 2n)$ cross sections by up to 100%. An average overall estimate

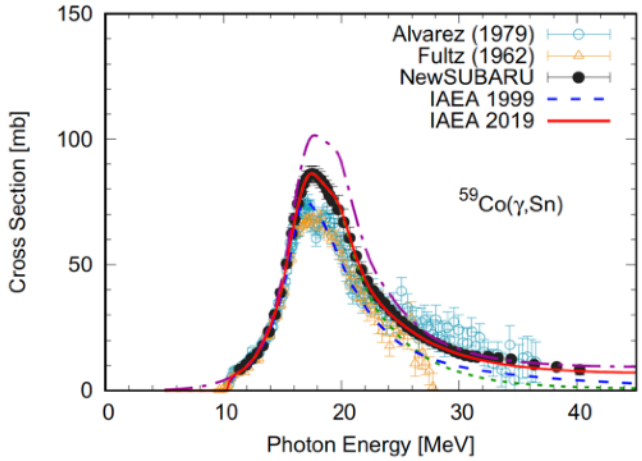

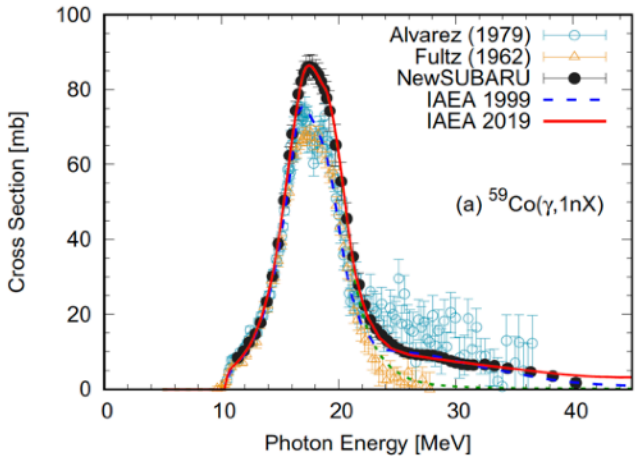

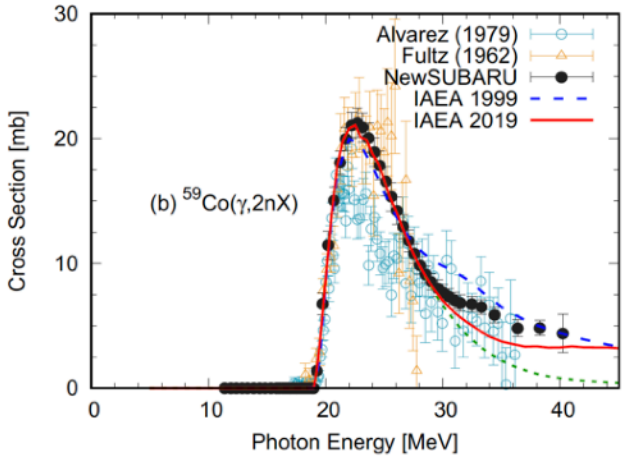

T. Kawano et al,. NDS163, 109 (2019)

Experimental Methods

NewSUBARU / GAKKO

NewSUBARU electron strorage ring

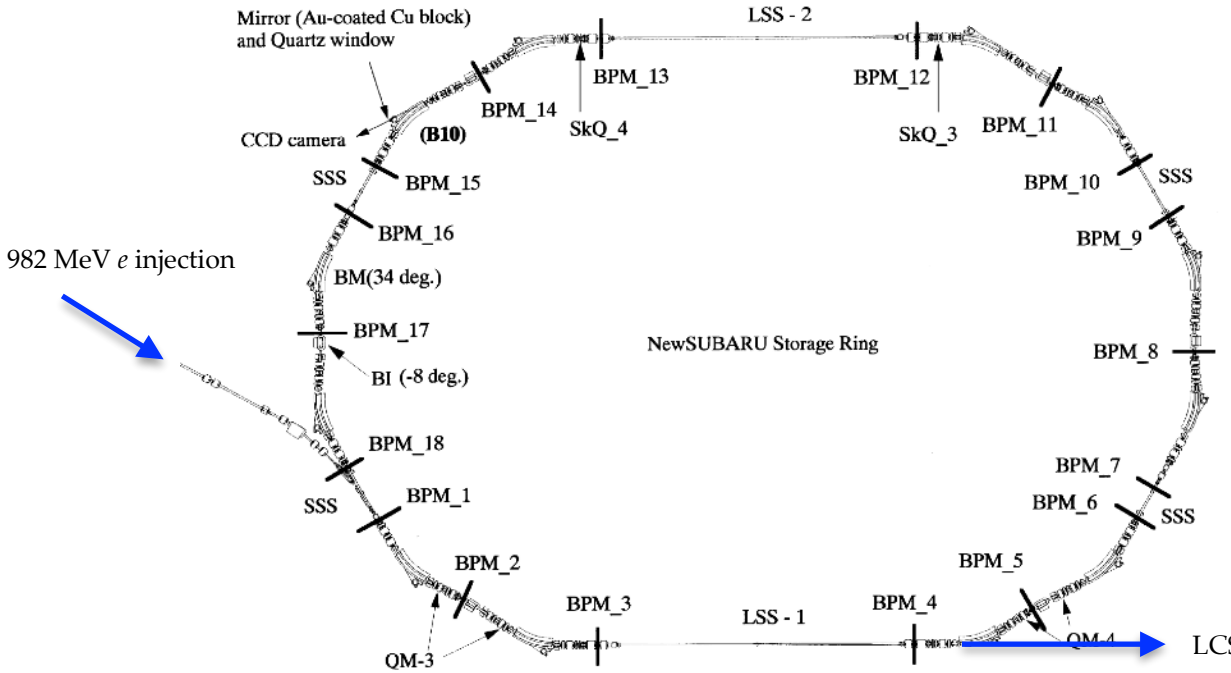

Fig. 1. Plane view of the newSUBARU ring.

Table 1
Present parameters of New SUBARU storage ring

Energy	1	GeV
Circumference L	118.731	m
Revolution frequency	2.525	MHz
Harmonic number	198	
RF frequency	~499.951	MHz
RF accel. voltage	138	kV
Betatron tunes	6.30/2.22	
α_p	0.00135	
Natural emittance	~38	nm
Natural energy spread	4.7×10^{-4}	
Straight sections	4 m	×4
	14 m	×2

1 - 1.5 GeV

A. Ando et al., J. Synchrotron Radiation 5, 342 (1998)

Y. Fukuda et al., NIMA 485, 805 (2002)

GACKO

(Gamma Collaboration Hutch of Konan University)

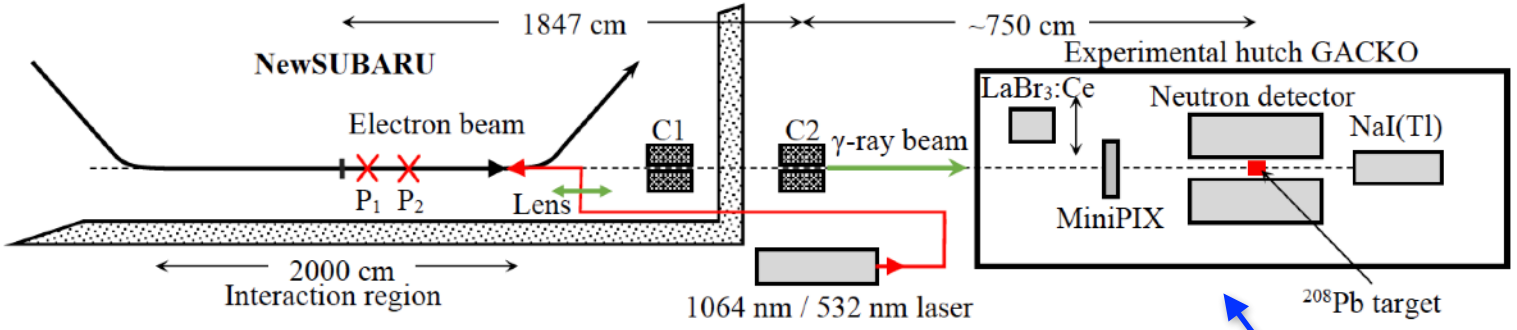

FIG. 1. Diagram showing the BL01 LCS γ-ray beam line and the experimental hutch GACKO at the NewSUBARU synchrotron radiation facility (not to scale). P_1 and the P_2 mark the focus point positions of the 1064 nm and, respectively the 532 nm laser beams at 1.8 and, respectively 3.8 m downstream of the eletron beam focus in the middle of the BL01.

LCS beam structure

fast time structure **60 ps** width, **500 MHz**, by electron bunch

slow time structure **20-40 ns** width, **1-20 kHz**, by laser pulse

beam: ON **80-90ms** / OFF **20-10 ms**
for background monitoring

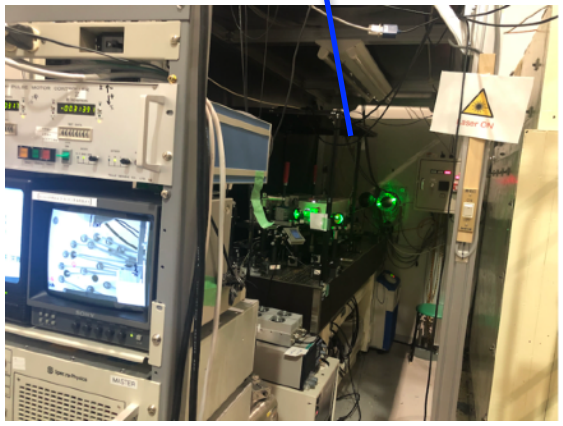

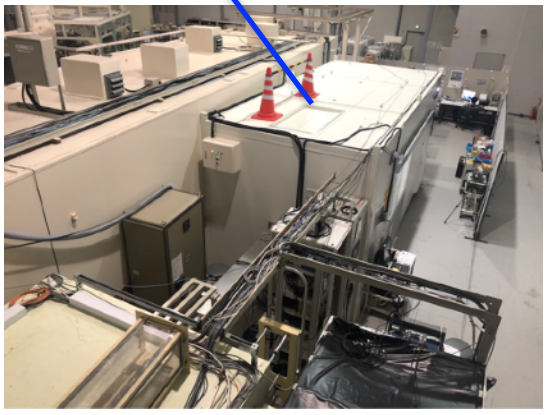

(photos by AT)

Gamma Beam Energy

e - beam: 650 - 1050 MeV

Laser: 1064 nm Nd:YVO4 INAZUMA laser
532 nm Talon (Diode-Pumped Solid State Q-Switched Lasers)

LCS γ : 7.5 - 38.1 MeV (85 steps)

$$E_\gamma = \frac{4\gamma^2 E_p}{1 + (\gamma\theta)^2 + 4\gamma E_p/(mc^2)}, \quad \sim 4\gamma^2 E_p \sim 4E_e^2 E_p$$

at 0 deg

Compton Scattering Energy

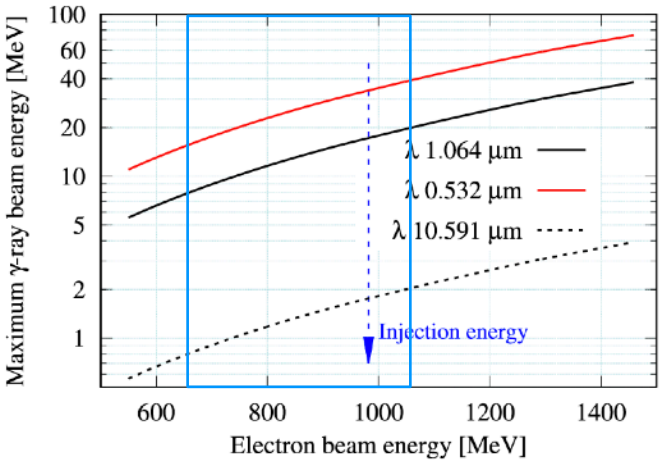

Fig. 4. Maximum energy of LCS γ-ray beams produced at NewSUBARU with the INAZUMA laser of λ = 1.064 μm, Talon laser of λ = 0.532 μm and CO_2 laser of λ = 10.59 μm.

D. Filipescu et al., NIMA 1047, 167885 (2023)

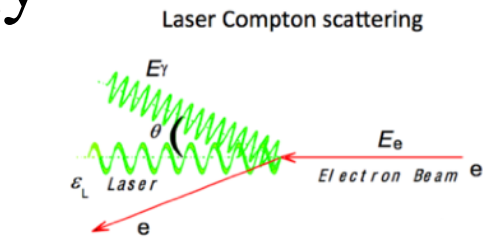

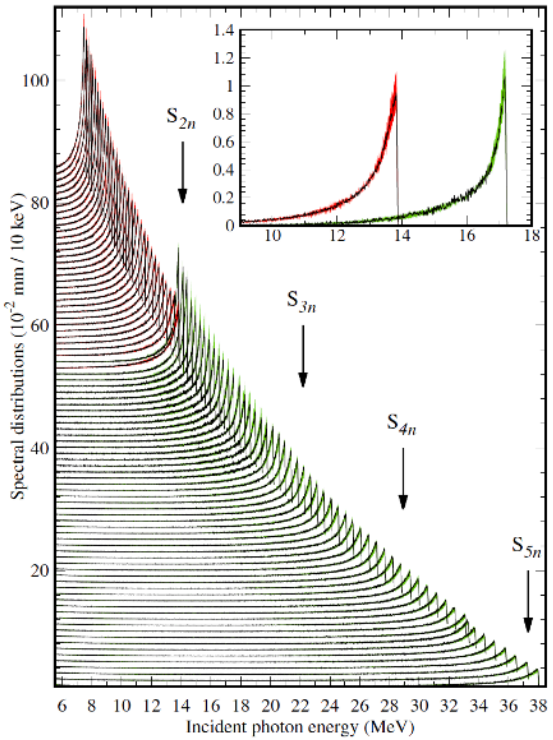

FIG. 2. The simulated energy profiles of the 85 incident LCS γ-ray beams used in the present experiment. Each curve is offset along the vertical axis for clarity. The spectral uncertainty is shown by the red band for γ beams obtained with the 1064 nm wavelength laser and by the green band for the ones obtained with the 532 nm laser. The inset shows the magnified spectra for the 13.86 and 17.21 MeV beams.

(present article)

Measurement Conditions (this article)

TABLE I. Parameters for the laser, electron and LCS γ-ray beams and measurement conditions. Z_R is the laser Rayleigh length [24], Δz is the longitudinal displacement between the focal positions of the laser and electron beams. f_{e-} is the RF frequency of the NewSUBARU storage ring. We give the pulse width of the 198 electron beam bunches circulating in the ring. E_m is the maximum energy of the γ-ray beam [22].

	(γ, n) neutron counting	(γ, in) multiplicity sorting
Laser beam:		
Laser	Inazuma	Talon
Wavelength (nm)	1064	532
Z_R (m)	0.57	6.1
Δz (m)	1.8	2.8
Power (W)	<40	<20
f_{laser} (kHz)	20	1
Pulse width (ns)	20	40
Beam on/off fill factor (%)	80	90
100% linear polarization perpendicular to accelerator plane		
Electron beam:		
E_{e-} (MeV)	651.30 – 887.65	649.29 – 1050.63
f_{e-} & pulse width	500 MHz & 60 ps	
Emittance $(\varepsilon_x, \varepsilon_y)$ (nm-rad):		
– nominal at injection	(38,1-3.8)	
– simulated	(50,5) – (70,7)	
LCS γ-ray beam:		
E_m (MeV)	7.50 – 13.86	13.84 – 38.02
Mean nb. of γ/pulse	5 – 14	6 – 20
Incident flux (γ/s)	$(8 - 22) \times 10^4$	$(0.5 - 1.8) \times 10^4$
ΔE_{FWHM} (MeV)	0.2 – 0.5	0.2 – 1.1
ΔE_{FWHM} (%)	2.7 – 3.9	1.6 – 3.1
Measurement conditions:		
Irradiation time (min)	5 – 30	~120
Target areal density (g/cm^2)	4.36	10.97

Beam flux monitor

NaI:Tl 8″ϕ-12″L

Pile-up spectrum fitting by Poisson distribution

→ average number of photons per laser pulse

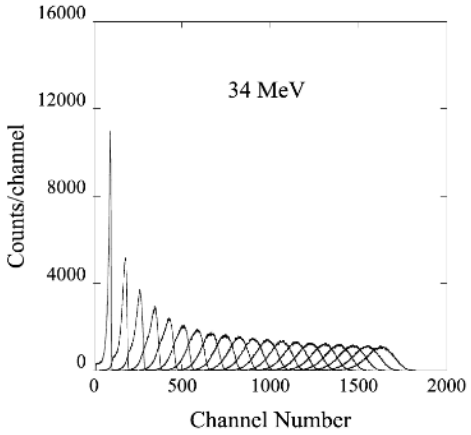

Fig. 4. Response functions to j-fold photons (j = 1, 2, 3, …, 20) at 34 MeV.

$$P_m(n) = \frac{m^n}{n!} e^{-m},$$

m: average number of photons per laser pulse

n: observed number of photons

P: probability for n with m

$$m^{exp} = \frac{\bar{N}_m}{\bar{N}_s},$$

$\bar{N}_m$: average channel for a multi photon spectrum

$\bar{N}_s$: average channel for a single photon spectrum

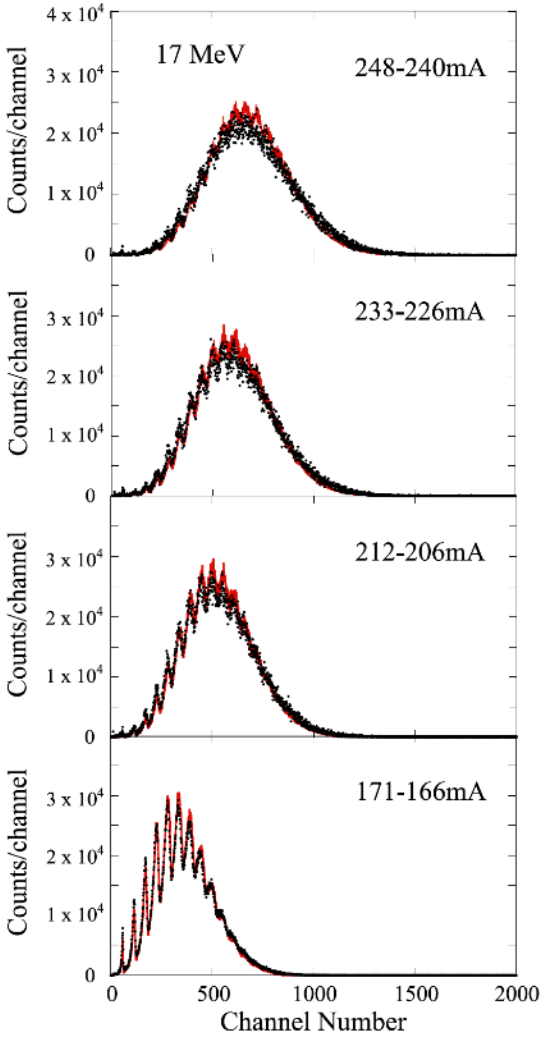

Fig. 6. (Color online) Experimental multi-photon spectra with time-variation at 17 MeV in comparison with the best-fit Poisson distributions.

H. Utsunomiya *et al.*, NIMA 896, 103 (2018)

Beam flux monitor

Test measurement of the photon flux & energy distribution

(photo by AT)

Target

Enriched metal powder

^{208}Pb 98.4%

8 mmϕ - 4 mm^{L}

for 7.5 MeV - S_{2n}

8 mmϕ - 6 mm^{L}

for S_{2n} - 38.1 MeV

Tin targets
(photo by AT)

TABLE II. ^{208}Pb separation energies for i neutrons S_{in} in MeV.

S_n	S_{2n}	S_{3n}	S_{4n}	S_{5n}
7.368	14.107	22.194	28.927	37.323

H. Utsunomiya *et al.*, NIMA 896, 103 (2018)

Neutron counting experiment

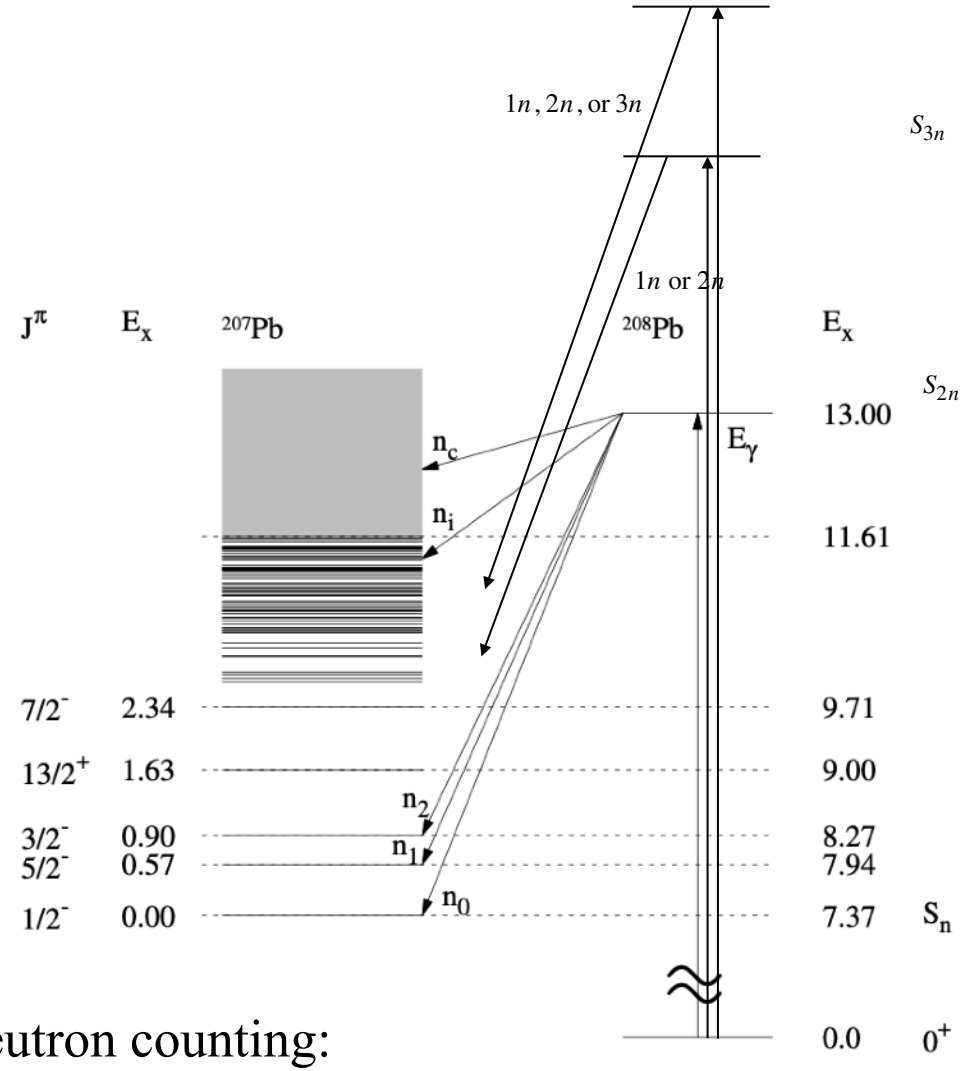

neutron counting:

Neutron Detection

^{3}He proportional counters: 10 atm 25 mmϕ - 450 mm^L

$$^3\mathrm{He} + n \rightarrow p + t$$

Flat-Efficiency Neutron Detector (FED)

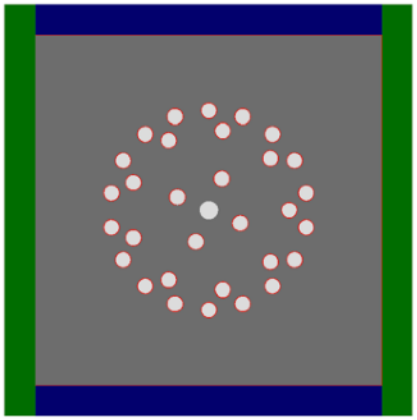

(photo by Tamii)

inner (4) and outer (9+18) rings of ^{3}He counters

$460^W \times 460^H \times 500^L$ mm^3

polyethylene moderator

H. Utsunomiya *et al.*, NIMA 871, 135 (2017)

Neutron Detection

Sum of the two rings
→ nearly flat efficiency

used for (γ, xn) cross sections

Ratio of the two rings
→ neutron energy dependence

used for n energy distribution

Simulations with
- monochromatic neutrons
and
- evaporation neutrons (Weisskopf-Ewing)

Conversion of RR to $\langle E_n \rangle$

including the uncertainty

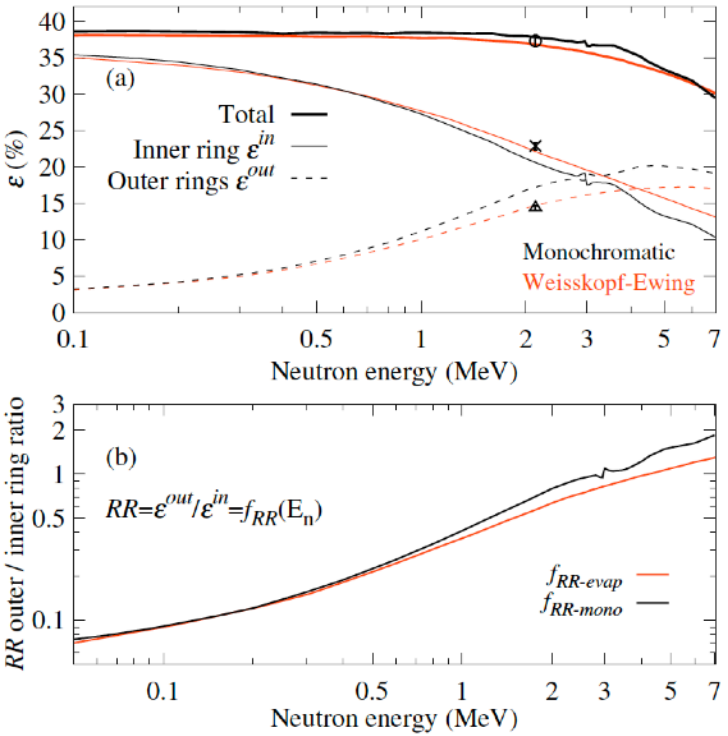

FIG. 3. FED calibration. (a) Experimental ^{252}Cf measurement for the total (circle), inner ring (cross) and summed outer rings (triangle) detection efficiencies reproduced by MCNP simulations for monochromatic neutrons (black) and evaporation neutron spectra (red). (b) The average neutron energy as function of the $\varepsilon^{in}/\varepsilon^{out}$ ratio between the efficiencies of the inner and summed outer rings of counters, here referred to as ring ratio functions f_{RR} and computed for both monochromatic and evaporation neutron spectra.

this article

Neutron Detection

neutron thermalization
→ arrival time distribution

black: beam on
red: beam off

background events during beam off:
neutrons from Bremsstrahlung photons by electron circulation
(and a small amount of cosmic rays)

background subtraction
dep. on arrival time

[19,20,32]

integration after b.g. subtraction

→ number of recorded neutrons in *i*-folded events

this article

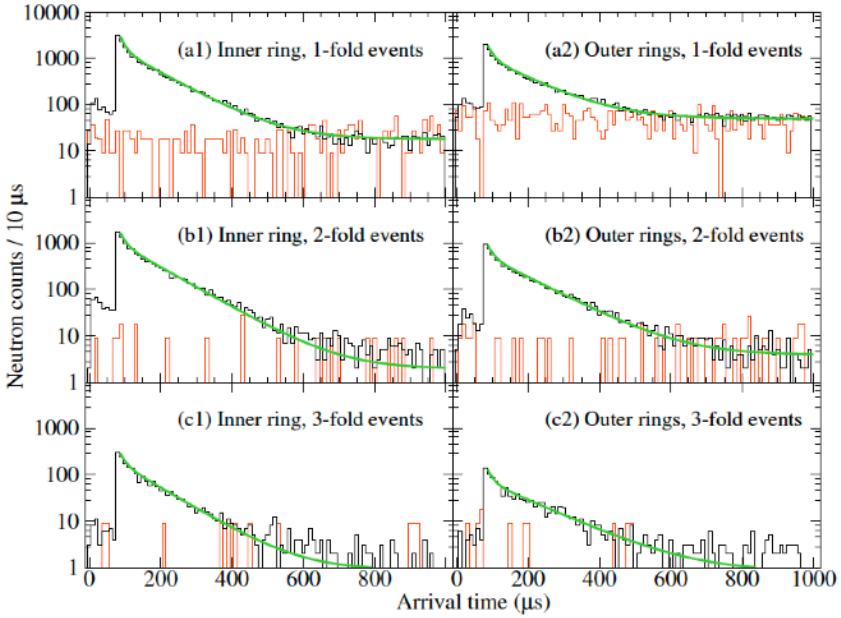

FIG. 4. Arrival time distributions of neutrons emitted in photoneutron reactions on ^{208}Pb at $E_\gamma = 27.72$ MeV $< S_{4n}$ and recorded by the (left) inner ring and (right) summed outer rings of ^{3}He counters. We plot separately the neutrons recorded in (a) 1-, (b) 2- and (c) 3-fold events. The black and red histograms correspond to beam-on and scaled beam-off data, respectively (see text). The green lines are fits to beam-on histograms.

Data Analysis

Events

inner ring	outer two rings
1-fold events	1-fold events
2-fold events	2-fold events
3-fold events	3-fold events
4-fold events	4-fold events
5-fold events	5-fold events

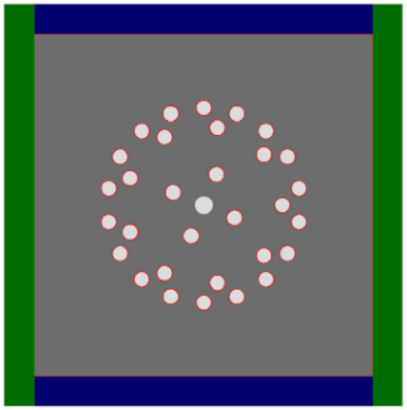

mutually exclusive

each of *in* and *out* rings

Neutron detection analysis procedure

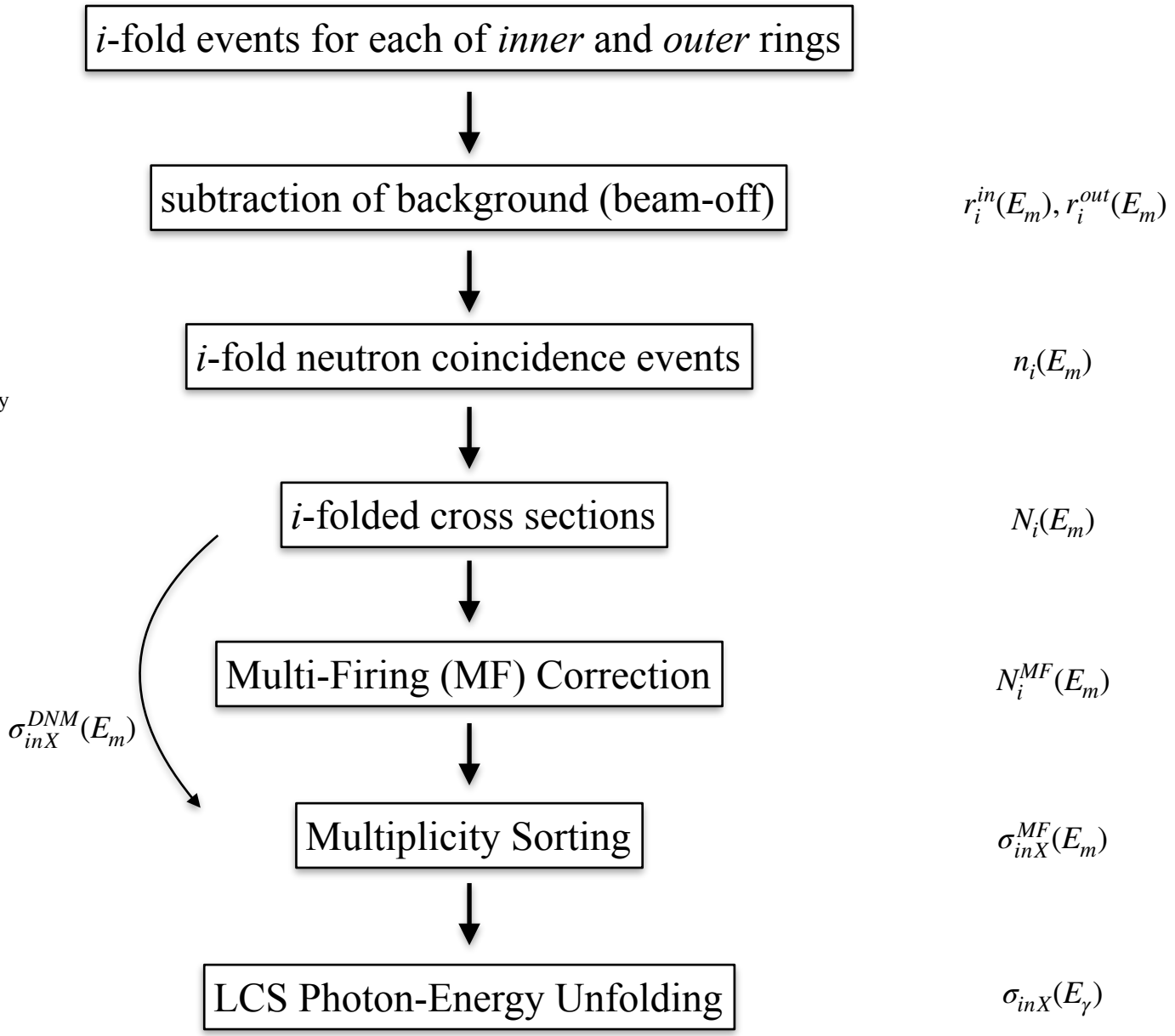

E_m : nominal LCS beam energy

E_γ : gamma energy

Neutron Coincidence Events

i-fold neutron coincidence events

$$n_i(E_m) = \frac{r_i^{out}(E_m) + r_i^{in}(E_m)}{i} \qquad (2)$$

E_m : LCS beam energy

$r_i^{in,out}(E_m)$: number of recorded neutrons in i-folded events
by integration of the b.g. subtracted time spectra

Neutron Coincidence Events

i-fold neutron cross section

$$N_i(E_m) = \frac{n_i(E_m)}{N_\gamma(E_m) n_T \xi(E_m)} \tag{3}$$

N_γ : number of incident photons

n_T : target number volume density

$\xi = \left[1 - \exp(-\mu L)\right]/\mu$: beam attenuation factor

$$\xi \equiv \frac{1}{I_0 L} \int_0^L I(z) dz \qquad I(z) = I_0 \exp\left(-\mu z\right)$$

Comment by AT

ξ must depend on each photon energy since μ depends on it.

Neutron Coincidence Events

i-fold neutron cross section

$$N_i(E_m) = \frac{n_i(E_m)}{N_\gamma(E_m) n_T \xi(E_m)} \qquad (3)$$

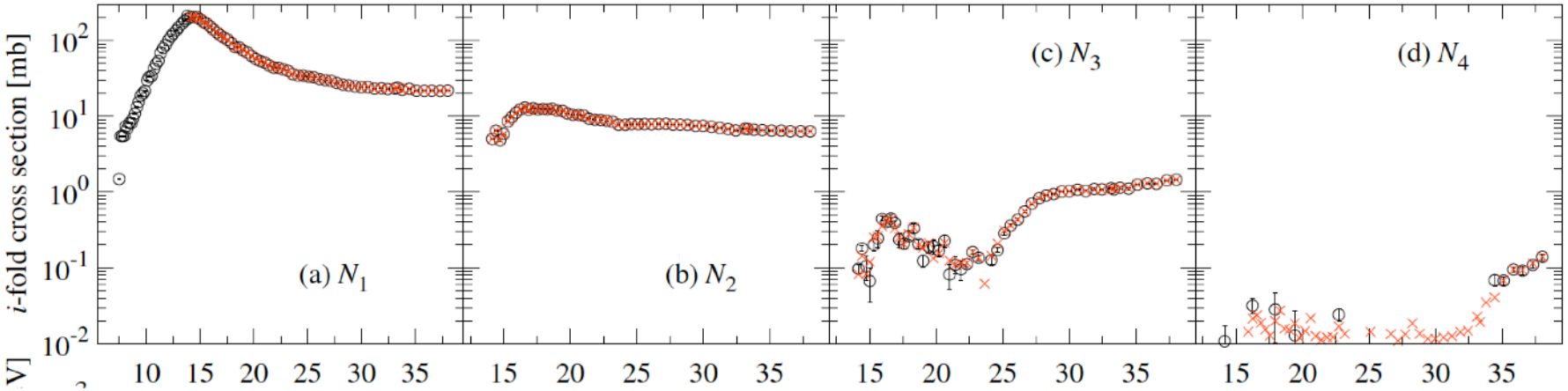

N_i : black open circles

N_i^{MF} : red crosses

Multi-Firing (MF)

There is a chance to have more than 1 reactions in a laser pulse.

This is called Multi-Firing (MF).

The MF effect is corrected by χ-square fitting procedure in Ref. [20]

$$N_i(i = 1...5) \rightarrow N_i^{MF}(i = 1...5)$$

$$\rightarrow \sigma_{inX}^{MF}$$

I. Gheorghe, et al., NIMA1019, 165867 (2021)

Neutron Multiplicity Sorting

j-fold neutron cross sections have contributions from j to $j_{\max}$-folded cross sections

$$N_j = \sum_{i=j}^{j_{\max}} \sigma_{inX} \cdot {}_iC_j \varepsilon^j (1-\varepsilon)^{i-j} \qquad (10)\ \text{modified}$$

※flat n efficiency (ε) against n energy is important

$$N_i \rightarrow \sigma_{inX}^{DNM}$$

$$N_i^{MF} \rightarrow \sigma_{inX}^{MF}$$

DNM=Direct Neutron Multiplicity Sorting

MF=Multi-Firing

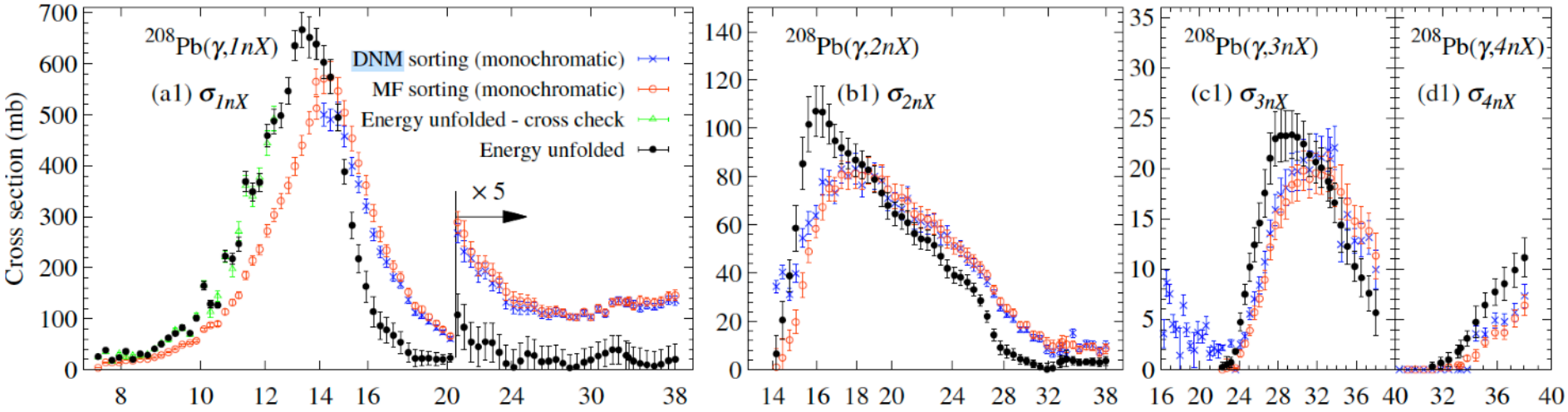

(LCS) Energy Unfolding

The observed cross section is the monochromatic cross section $\sigma_{inX}(E_\gamma)$ folded by the LCS photon energy spectrum $L(E_\gamma, E_m)$.

$$\sigma_{inX}^{MF}(E_m) = \frac{1}{\xi}\int_0^{E_m} L(E_\gamma, E_m)\sigma_{inX}(E_\gamma)dE_\gamma \qquad (12)$$

Unfolding by χ^2 fitting (using CERN MINUIT).

$$\rightarrow \sigma_{inX}(E_\gamma)$$

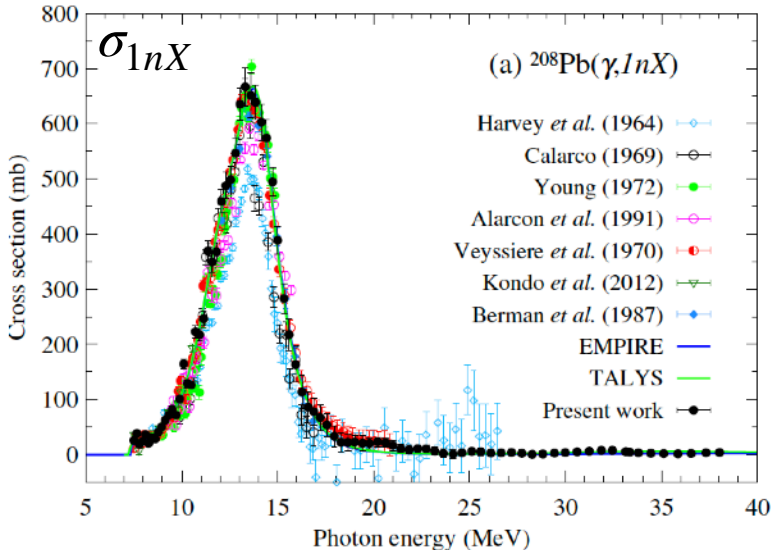

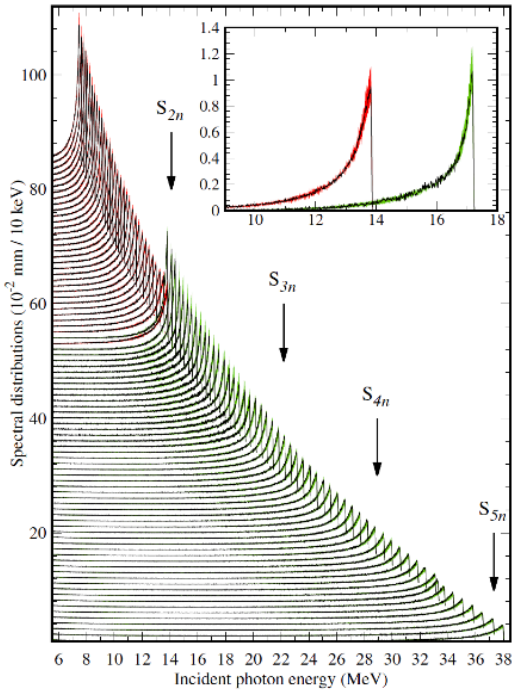

FIG. 2. The simulated energy profiles of the 85 incident LCS γ-ray beams used in the present experiment. Each curve is offset along the vertical axis for clarity. The spectral uncertainty is shown by the red band for γ beams obtained with the 1064 nm wavelength laser and by the green band for the ones obtained with the 532 nm laser. The inset shows the magnified spectra for the 13.86 and 17.21 MeV beams.

I. Gheorghe, et al., NIMA1019, 165867 (2021)

Neutron Energy Analysis

RING Ratio

$$RR_i = \frac{r^{out}(E_m)}{r^{in}(E_m)}$$

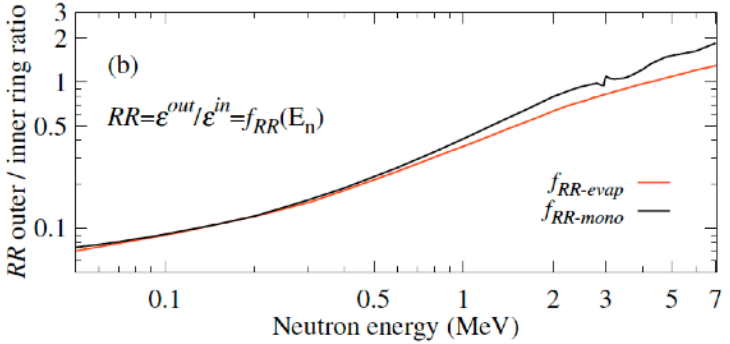

average neutron energy

$$E_i^{exp} = f_{RR-evap}^{-1}(RR_i)$$

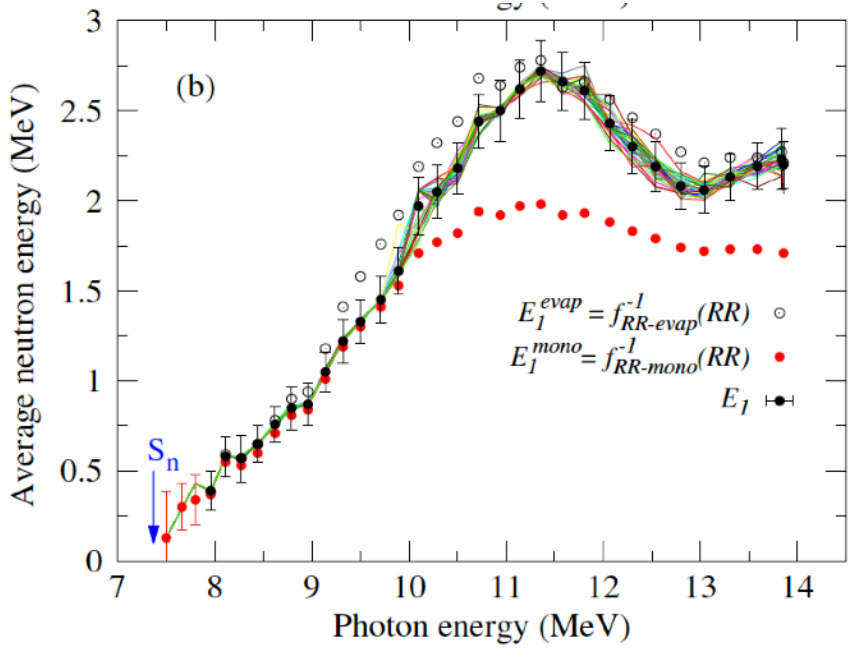

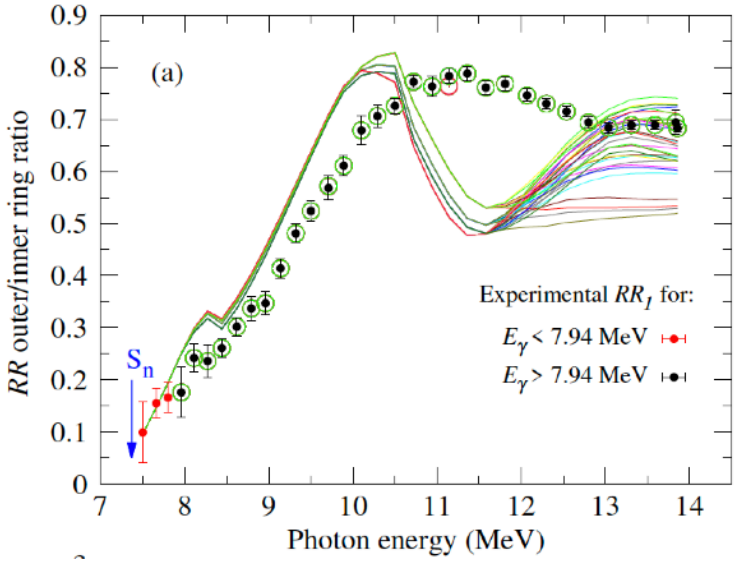

Neutron Energy Spectrum below S_{2n}

χ^2 fit of neutron energy distribution assuming statistical decay and level density, etc.

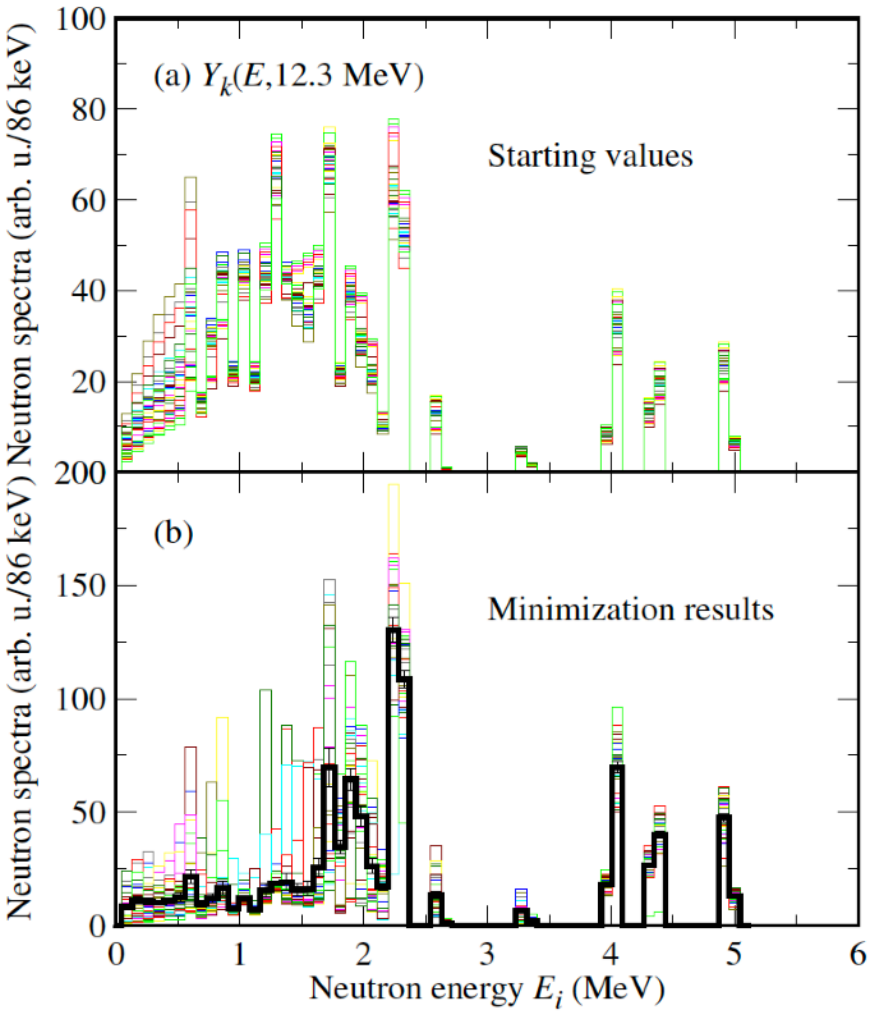

$E_\gamma = 12.3$ MeV

Neutron Energy Spectrum below S_{2n}

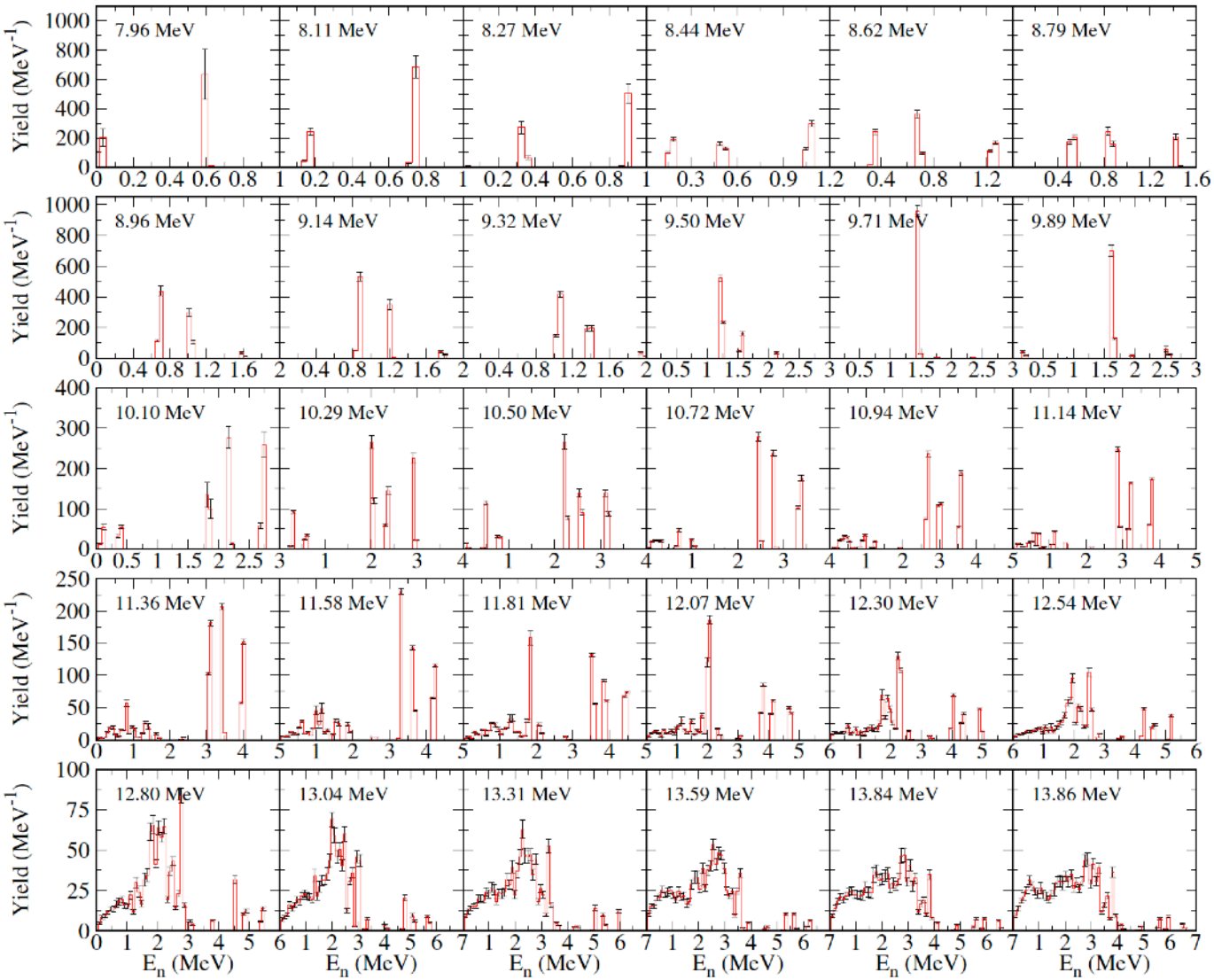

FIG. 14. Present estimations for the ^{208}Pb(γ, n) photoneutron spectra normalized to an integral of 1000 counts for incident photon energies up to 13.86 MeV.

Neutron Multiplicity Sorting

$$N_j = \sum_{i=j}^{j_{\max}} \sigma_{inX} \cdot {}_iC_j \varepsilon^j (1-\varepsilon)^{i-j} \qquad (10) \text{ modified}$$

$$E_j = \frac{1}{N_j} \sum_{i=j}^{j_{\max}} E_{inX} \sigma_{inX} \cdot {}_iC_j \varepsilon^j (1-\varepsilon)^{i-j} \qquad (11) \text{ modified}$$

$$N_i \rightarrow E_{inX}^{DNM}$$

$$N_i^{MF} \rightarrow E_{inX}^{MF}$$

(LCS) Energy Unfolding

$$\sigma_{inX}^{MF}(E_m) = \frac{1}{\xi}\int_0^{E_m} L(E_\gamma, E_m)\sigma_{inX}(E_\gamma)dE_\gamma \qquad (12)$$

$$E_{inX}^{MF}(E_m) = \frac{1}{\xi\sigma_{inX}^{MF}(E_m)}\int_0^{E_m} L(E_\gamma, E_m)\sigma_{inX}(E_\gamma)dE_\gamma \qquad (13)$$

Unfolding by χ^2 fitting (using CERN MINUIT).

$\rightarrow E_{inX}(E_\gamma)$

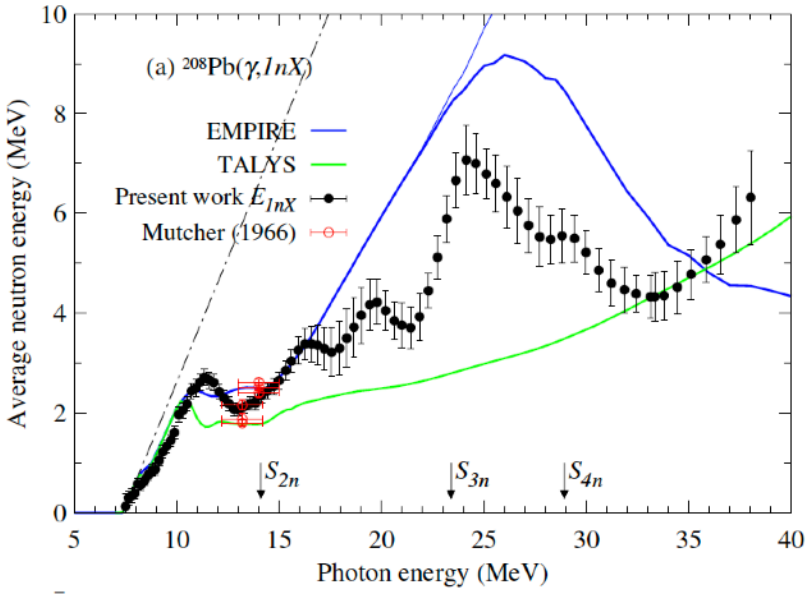

Results

Photo-absorption Cross Section

Photo-absorption Cross Section

$$\sigma_{abs} \simeq \sum_i \sigma_{inX}$$

Good agreement with
- Saclay (Veyssiere)

and

- RCNP (Tamii)

- Livermore (Harvey)

is significantly small

- Livermore (Berman)

is 5% smaller at the peak

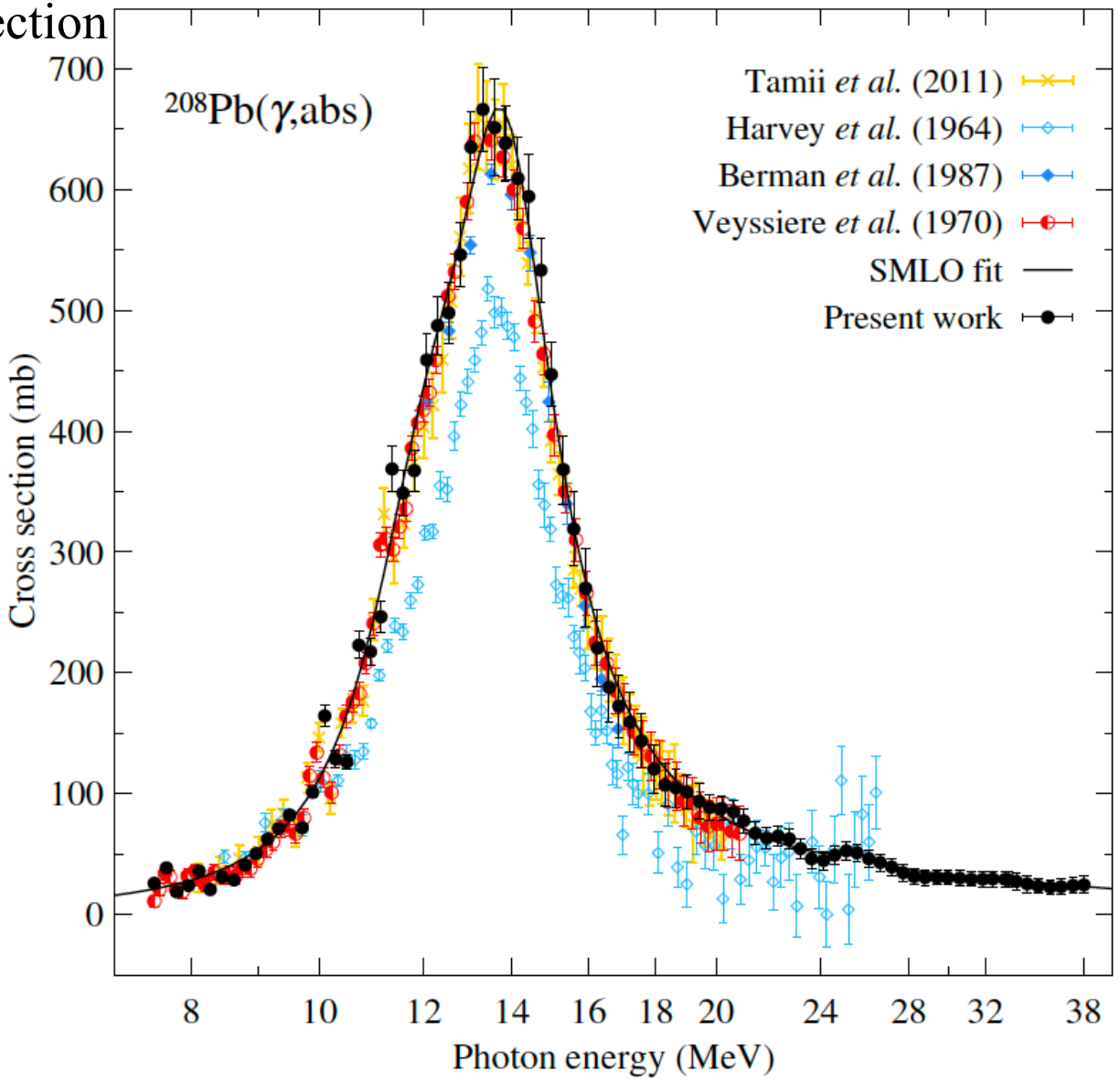

Photo-neutron Cross Sections

Photo-neutron Cross Sections

σ_{inX}

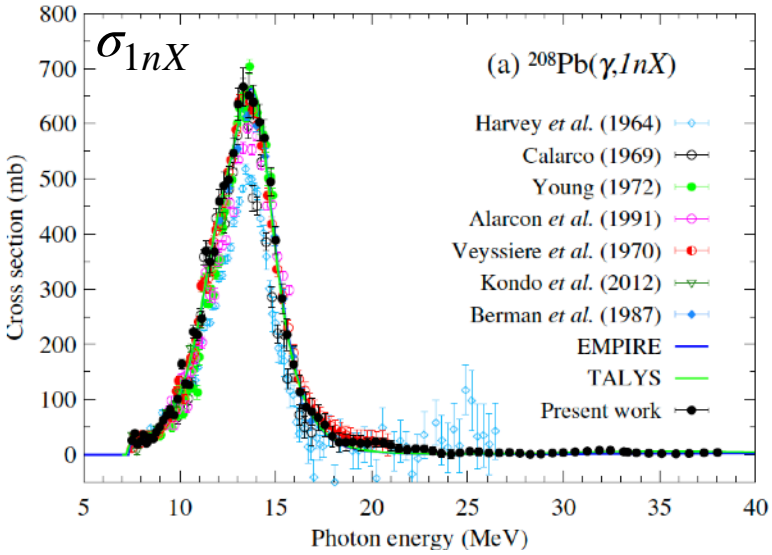

Good agreement with
- Saclay (Veyssiere)
- Kondo (LCS)
- Young (Tagged-Brems) at peak region
- Calarco at lower energy tail

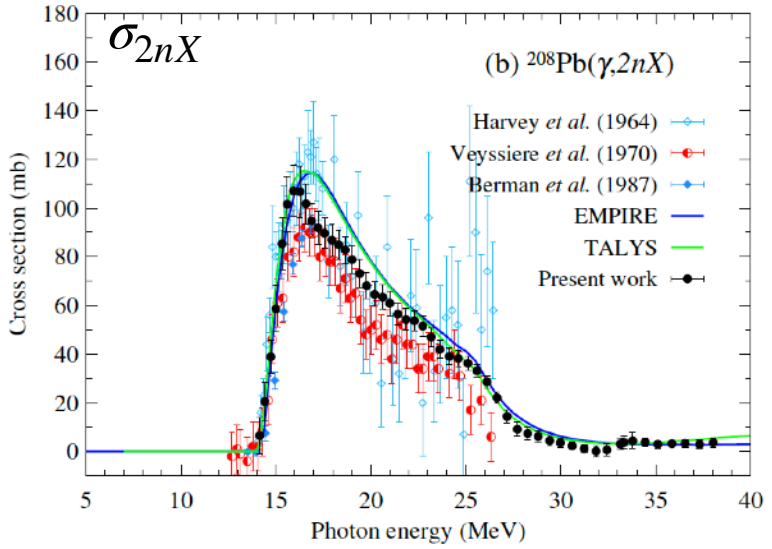

Higher than
- Saclay (Veyssiere)
- Livermore (Berman)

Better Agreement with
- Saclay (Harvey)

Photo-neutron Cross Sections

Photo-neutron Cross Sections

σ_{inX}

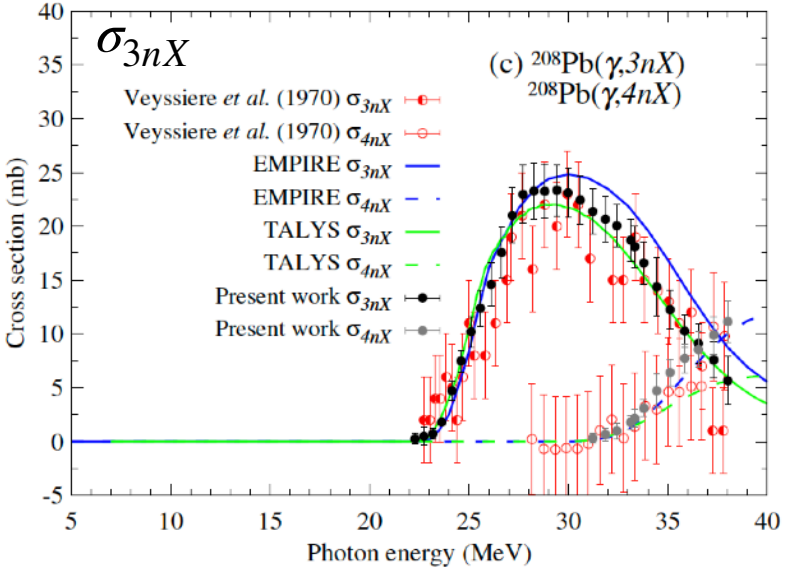

In agreement with
- Saclay (Veyssiere)

Integrated Values

- the integrated cross section Σ_{TRK} defined in terms of the Thomas-Reiche-Kuhn (TRK) sum rule $\sigma_{TRK} = 60NZ/A$ mb MeV, *i.e.*

$$\Sigma_{TRK} = \frac{1}{\sigma_{TRK}} \times \int_0^\infty \sigma_{abs}(\omega) d\omega \qquad (15)$$

- the centroid energy

$$E_c = \frac{\int_0^\infty \sigma_{abs}(\omega) d\omega}{\int_0^\infty \sigma_{abs}(\omega)/\omega \; d\omega} \qquad (16)$$

- and the polarizability

$$\alpha_D = \frac{\hbar c}{2\pi^2 e^2} \int_0^\infty \frac{\sigma_{abs}(\omega)}{\omega^2} d\omega \; . \qquad (17)$$

TABLE IV. ^{208}Pb experimental integrated cross section Σ_{TRK}, centroid energy E_c, and polarizability with their estimated uncertainties (Err) on the basis of the present measurements and comparison with the values obtained in Ref. [6]

	Present	Ref. [6]
Σ_{TRK}	1.27 ± 0.10	1.29 ± 0.03
E_c [MeV]	14.20 ± 0.12	14.53 ± 0.29
α_D [fm$^3/e^2$]	20.00 ± 1.30	19.82 ± 0.49

from RCNP Data

TABLE III. ^{208}Pb GDR parameters adopted within the SMLO model for the three Lorentzians. σ corresponds to the peak cross section, E to the centroid energy and Γ to the full width at half maximum. i is the Lorentzian index.

i	$\sigma^{(i)}_{\mathrm{GDR}}$ (mb)	$E^{(i)}_{\mathrm{GDR}}$ [MeV]	$\Gamma^{(i)}_{\mathrm{GDR}}$ [MeV]
1	260.65	12.20	3.251
2	526.13	13.93	3.06
3	8.44	25.56	1.97

Neutron Energy Spectra

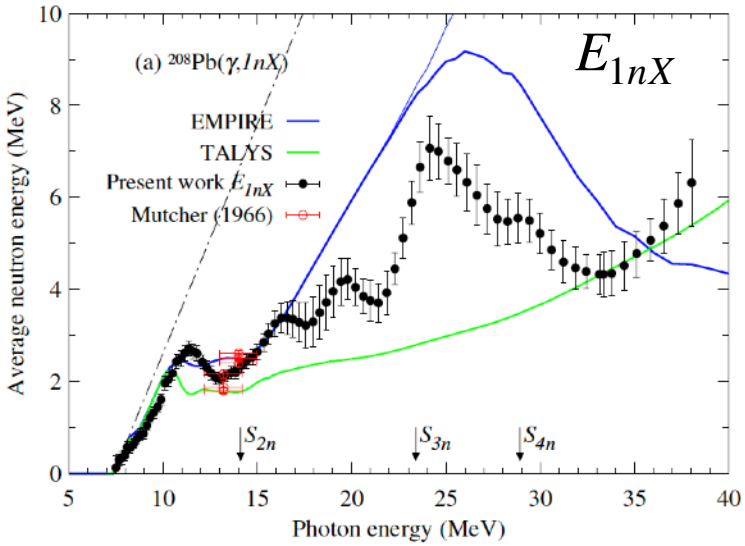

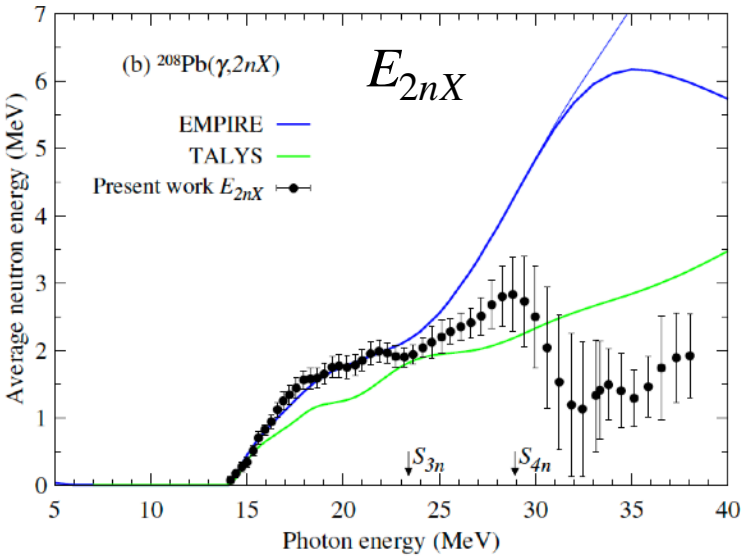

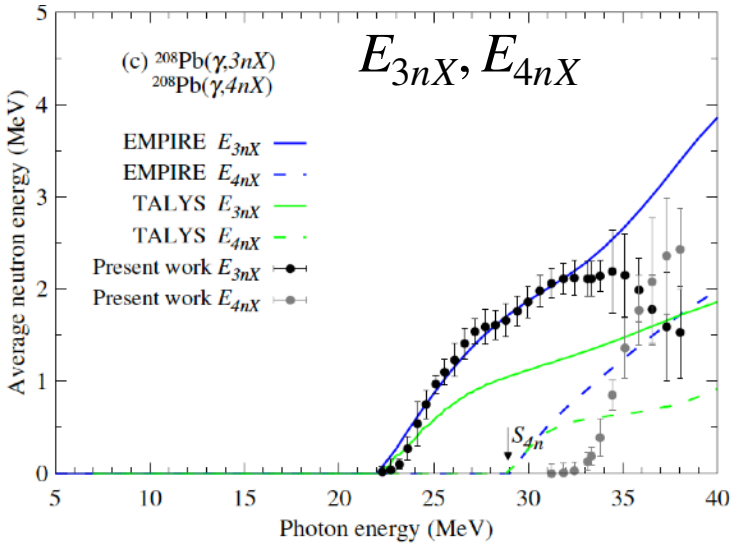

1n partial cross sections

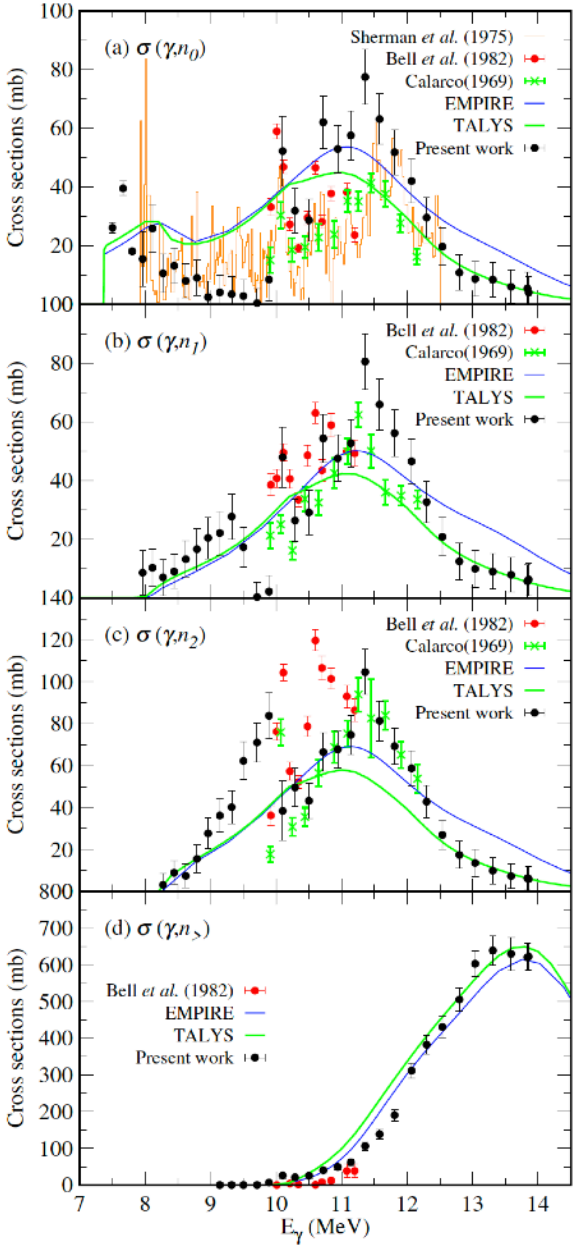

Fine Structure at the lower energy tail of IGVDR

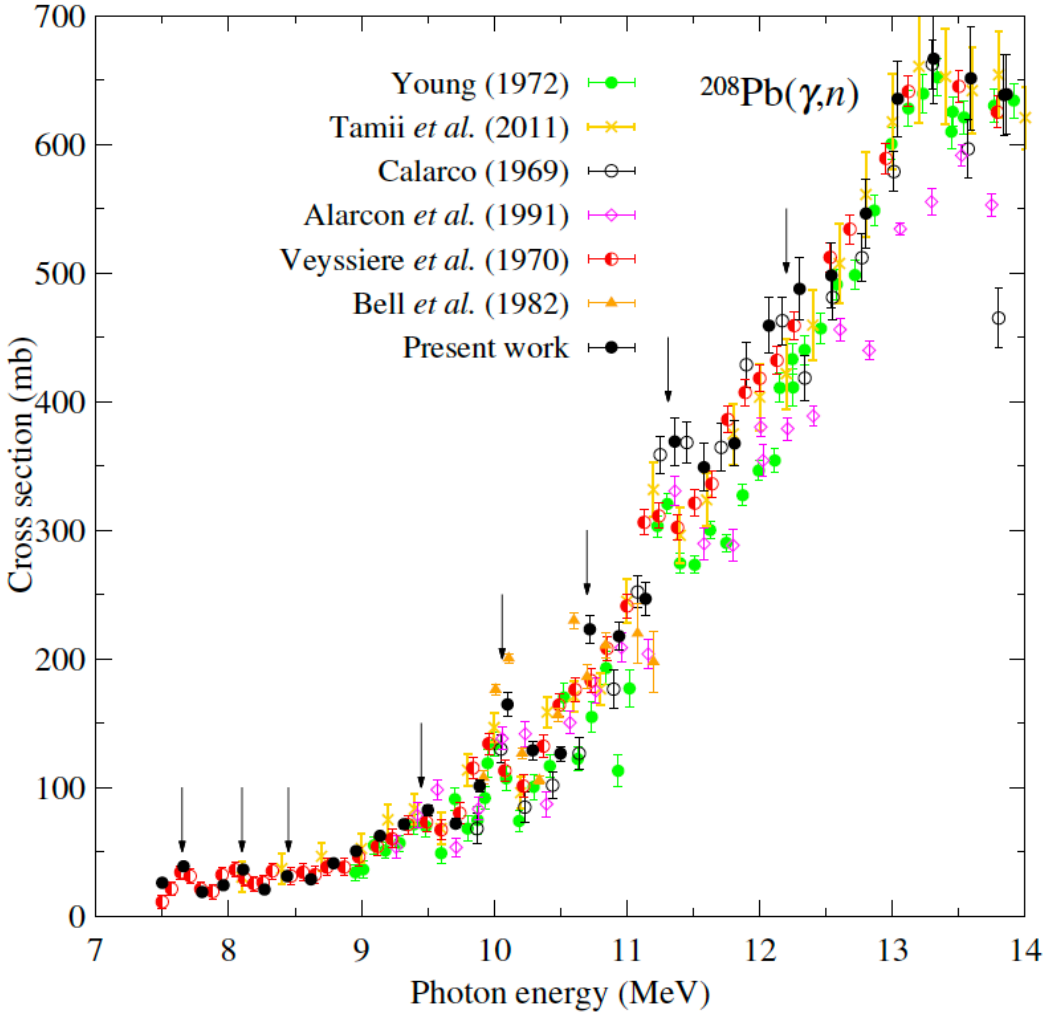

- Peaks at 7.65, 8.10 and 8.45
  consistent with Saclay
- Broad structure at 9.45
  similar to Saclay and RCNP
- Structure at 10 MeV
  consistent with tagged-brems (Bell)
  consistent with Alarcon
  150 keV higher Saclay
- Peak 10.7 MeV
  consistent with BLL
  RCNP observed as a sholder
- Peak at 11.3 MeV
  consistent with tagged-brems
  100 keV higher than Saclay and RCNP
- Peak at 12.2 MeV
  also observed in other experiments

RCNP Data

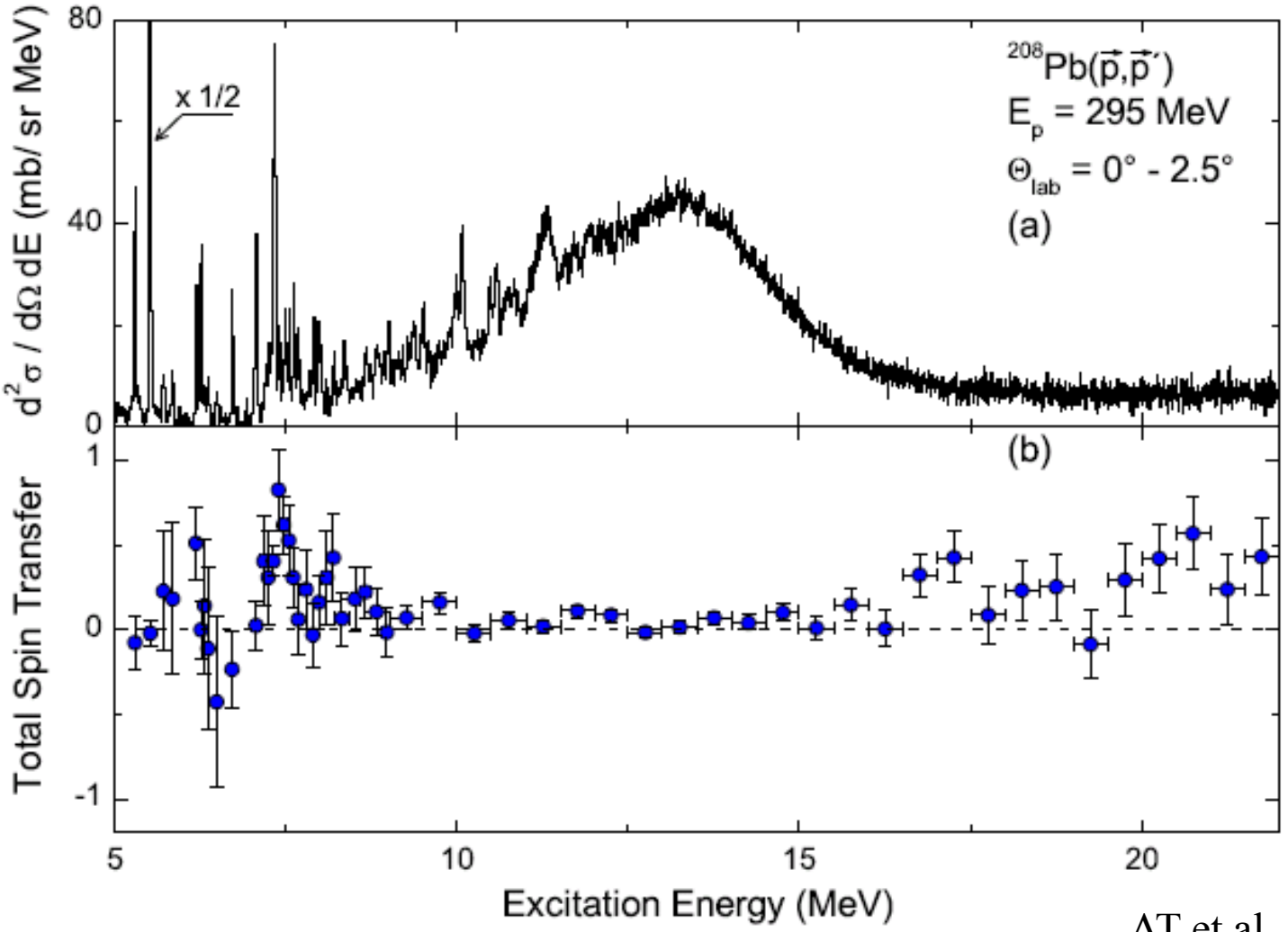

AT et al., PRL2011

$$\text{Total Spin Transfer } \Sigma \equiv \frac{3-(2D_{SS}+D_{LL})}{4} = \begin{cases} 1 \text{ for } \Delta S = 1 & \text{spin-M1} \\ 0 \text{ for } \Delta S = 0 & \text{E1} \end{cases}$$

RCNP Data

folded with the LCS gamma spectra
assuming only the *E1* c.s.

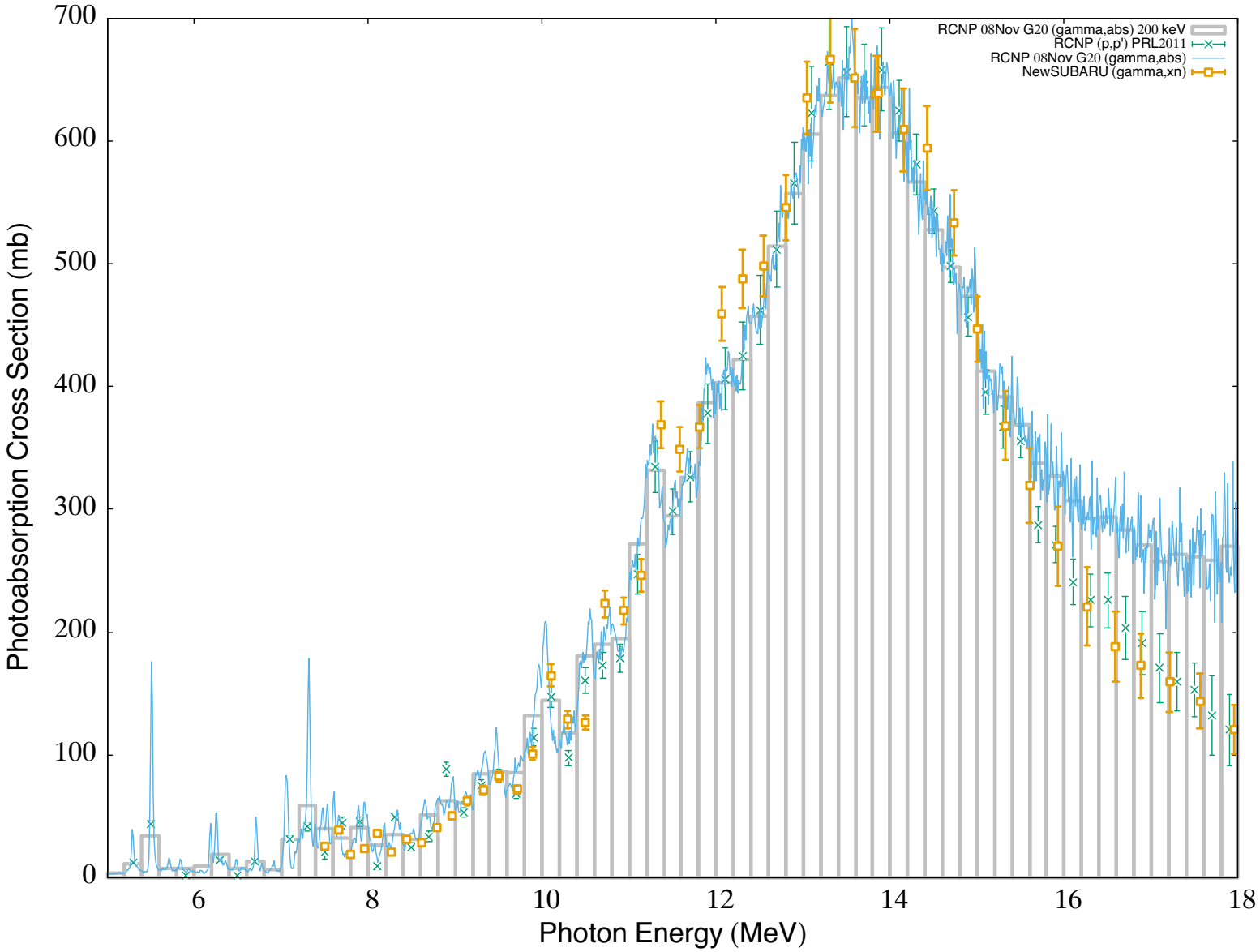

RCNP Data

folded with the LCS gamma spectra
assuming only the *E1* c.s.

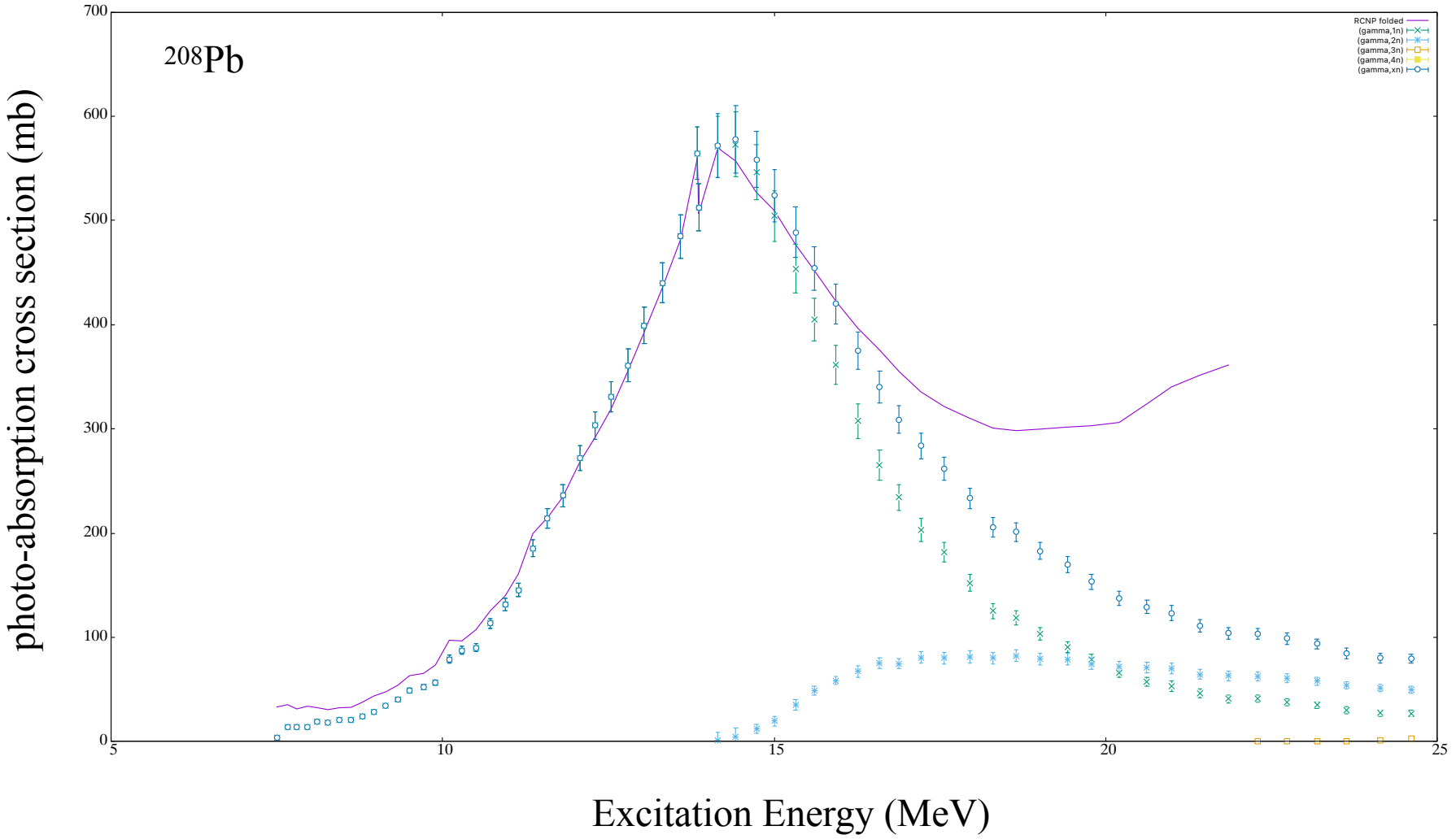

RCNP Data

folded with the LCS gamma spectra
assuming only the *E1* c.s.

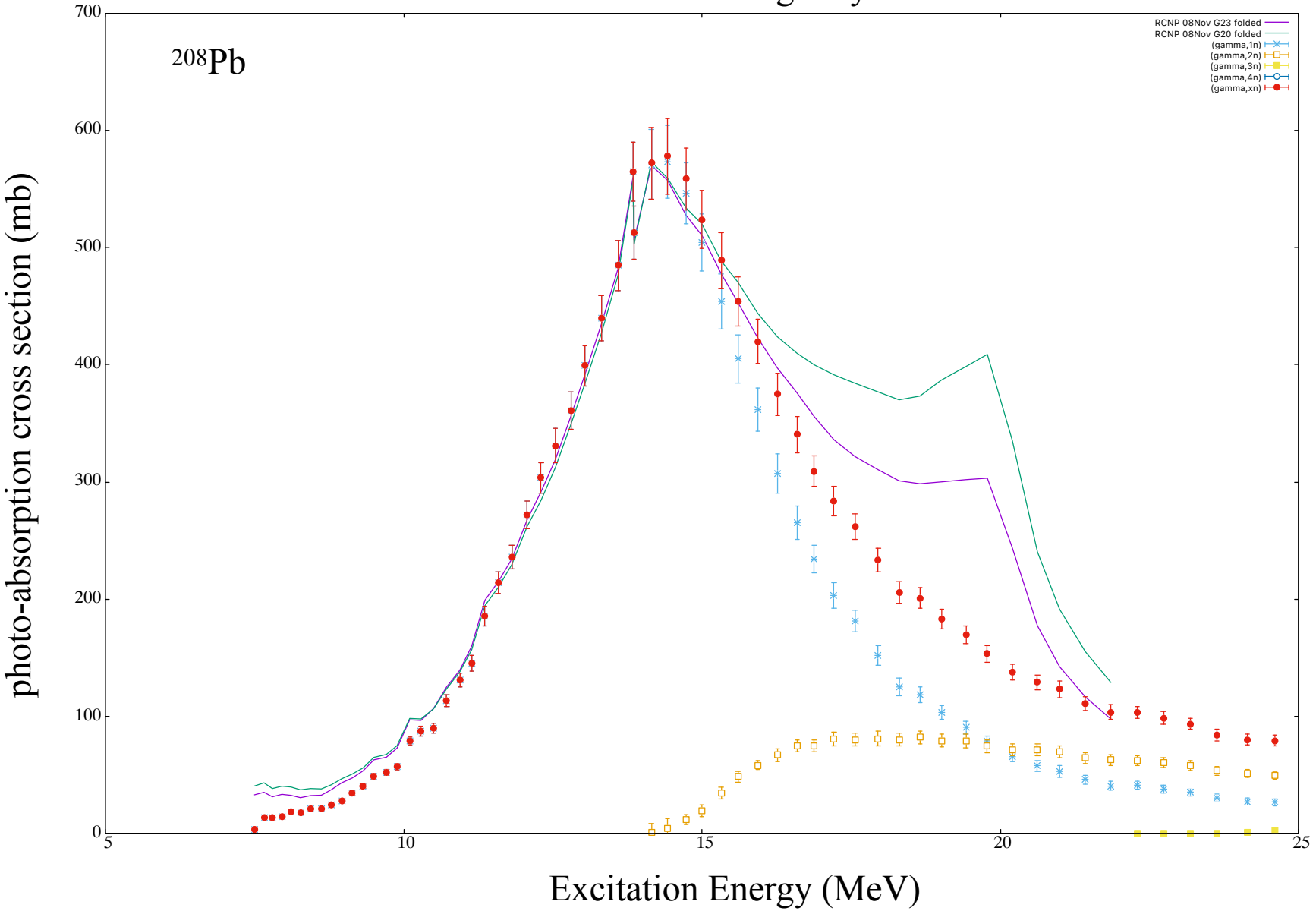

Summary

We obtained the cross sections for the $(\gamma, 1nX)$, $(\gamma, 2nX)$, $(\gamma, 3nX)$ and $(\gamma, 4nX)$ photoneutron reaction channels. The photoabsorption cross sections, extracted as the sum of the photoneutron cross sections, confirm the Saclay results of Ref. [9]. The present experiment extended the area of investigation of the photoabsorption excitation function above the maximum limit of 21 MeV reached in the Saclay experiment. Fine structures have been observed in the $^{208}\mathrm{Pb}(\gamma, n)$ reaction at incident energies lower than 13 MeV and compared with previous high resolution measurements. Average energies of neutrons emitted in each reaction have also been extracted based on the ring ratio data. Low average energies for the $(\gamma, 1nX)$ and $(\gamma, 2nX)$ neutrons at excitation energies above S_{3n} indicate a significant contribution of charged particle emission reactions. The experimental photoneutron cross sections and average energies have been satisfactorily reproduced with both EMPIRE and TALYS calculations by slight adjustments of model parameters.

Summary

Based on the measured ring ratio values, we have extracted estimations on the total neutron emission spectra in the ^{208}Pb(γ, n) reaction at incident energies lower than S_{2n}, which confirm a gradual transition from discrete energy neutron emission to a statistical neutron emission towards S_{2n}. Present estimations for the partial photoneutron cross sections for populating the ^{207}Pb residual in its ground and first two excited states reproduce the resonant structures observed in the previous experiments and significantly extend the previously investigated energy range. Until detailed time of flight measurements are available, such systematic estimations on a wide energy range are useful for microscopic descriptions of the GDR structure.

Finally, the $E1$ moments extracted from the present data are in rather good agreement with those obtained from the previous measurement of Ref. [10] and confirm the mysterious kink previously found between ^{208}Pb and ^{209}Bi polarizabilities in Ref. [6].